The Oxygen Reduction Reaction in Non-aqueous Electrolytes: Li-Air Battery Applications.

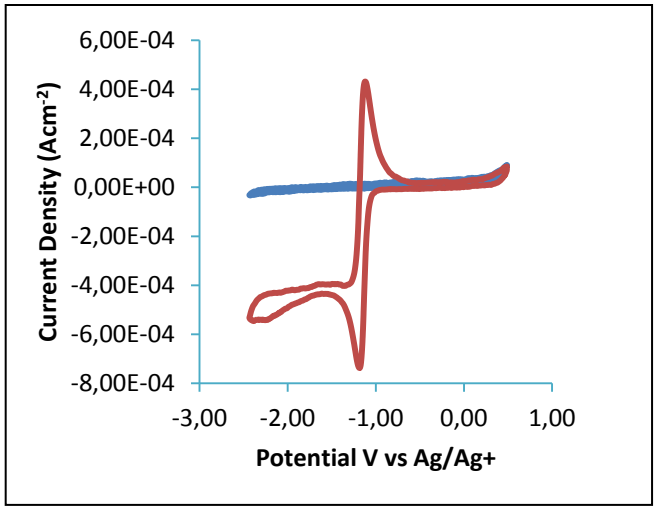

MD. KHAIRUL HOQUE

Degree project for Master of Science 30 hec

Department of chemistry and Molecular Biology
Electrochemistry Group
University of Gothenburg

Faculty of Science

UNIVERSITY OF GOTHENBURG

2013/09

The Oxygen Reduction Reaction in Non-aqueous Electrolytes: Li-Air Battery Applications

MD. KHAIRUL HOQUE

Department of Chemistry and Molecular Biology
Electrochemistry Group
University of Gothenburg
Gothenburg, Sweden, 2013

Abstract

Lithium air battery is one of the most promising power technologies of future because it has theoretical specific energies 100 times that of the state of the art Li-ion battery. One of the main obstacles in the development of Li-air battery technology is the stability of electrolyte. The focus of research work presented in this thesis is on the investigation of the oxygen reduction reaction (ORR) in non-aqueous electrolytes relevant for Li-air batteries. The oxygen reduction reaction mechanisms and kinetics are elucidated by using the electrochemical techniques such as cyclic voltammetry. Dimethyl sulfoxide (DMSO) and acetonitrile (MeCN) were chosen as solvents whereas tetrabutylammonium hexafluorophosphate ($TBAPF_6$), lithium perchlorate $LiClO_4$ and lithium hexafluorophosphate ($LiPF_6$) as supporting electrolytes. By using the glassy carbon electrode as working and platinum mesh as counter electrode it was found that the ORR is quasi-reversible in $TBAPF_6$/DMSO as well as in $TBAPF_6$/MeCN. In the case of lithium based supporting electrolytes ($LiPF_6$ and $LiClO_4$) the ORR in DMSO as well as MeCN was irreversible with a follow-up chemical reaction. These results show that the interaction of small highly charged Li^+ with surrounding solvent and counter ions is markedly different than large bulky TBA^+ ion and such interactions strongly affect the reaction mechanism of oxygen reduction and oxygen mobility through the electrolytes. Moreover, the differences seen in the reversibility of the ORR in TBA^+ compared with Li^+ containing electrolytes is probably due to the formation of insulating Li_2O/Li_2O_2 on cathode during the discharging process. The knowledge of the ORR mechanism inferred from these results will be useful for the selection of appropriate organic electrolytes and for a rapid development of the rechargeable Li-air battery for automotive industry.

Key words: Cyclic voltammetry (CV) and rotating disk voltammetry (RDE), the oxygen reduction reaction (ORR).

Table of content

Chapter1

1.1. Motivation and aim of the study

This project is a part of a big project ‘’Testing and Exploration of Metal Air Battery Technology’’. The metal air battery technology is quite new for Swedish automotive industries. The whole project consists of different parts such as literature survey of the different metal air technologies, modeling of metal air cell, fundamental understanding of electrode reaction mechanisms, construction of Swagelok design Li-air cell and preliminary testing of available metal air batteries. A vital part of the project is related with the studies of reaction mechanisms of Li-air battery. The results from this project will further be used in performing simulations of full Li-air cell.

The aim was to gain fundamental understanding of oxygen reduction reactions by using the electrochemical techniques. Non-aqueous based Li–air system was chosen due to its advantage over aqueous system. Literature survey was done to find most appropriate organic solvents and salts currently used in Li-air battery systems. DMSO and MeCN were found as good solvents because they have shown good results compared with other solvents. Therefore DMSO and MeCN were chosen for further studies of reaction kinetics (1). Electrochemical techniques such as cyclic voltammetry (CV) and Rotating Disk Electrode (RDE) were used to elucidate the kinetics of these reactions.

1.2 Introduction

1.2.1. Overview of Li-air battery

Lithium air battery is usually defined as a battery consists of Lithium metal-based anode and porous carbon based air-cathode, which continuously extracts oxygen from air (2). Current Li-ion batteries are not satisfactory for the practical application of electric vehicles, because of their electrode materials having intercalation chemistry. Solvent co-intercalated into graphite cathode. Electric vehicles need high current supply and this problem is more in high current application. Therefore, Li-air batteries have received significant attraction due to

their energy density, which is higher than current Li-ion battery. Li-air batteries can be categorized based on the type of electrolyte used,

i) Aprotic (organic) solvents

ii) Aqueous solvents

iii) Hybrid (non-aqueous/aqueous) solvents, and

iv) All solid-state electrolyte.

A typical design for non-aqueous or aprotic lithium air batteries is shown in figure 1a, which is composed of a metallic lithium anode, lithium salt in an organic solvent, and a porous O_2 breathing cathode composed of large surface area carbon particles and catalyst particles. The most common technique of preparing cathode materials for non-aqueous system is to mix carbon black (Ketjen Black, active coal), a polymer binder and an organic solvent to form slurry which is coated on a metal grid. The resulting air cathode should have higher surface area with reasonable pore volume (3).

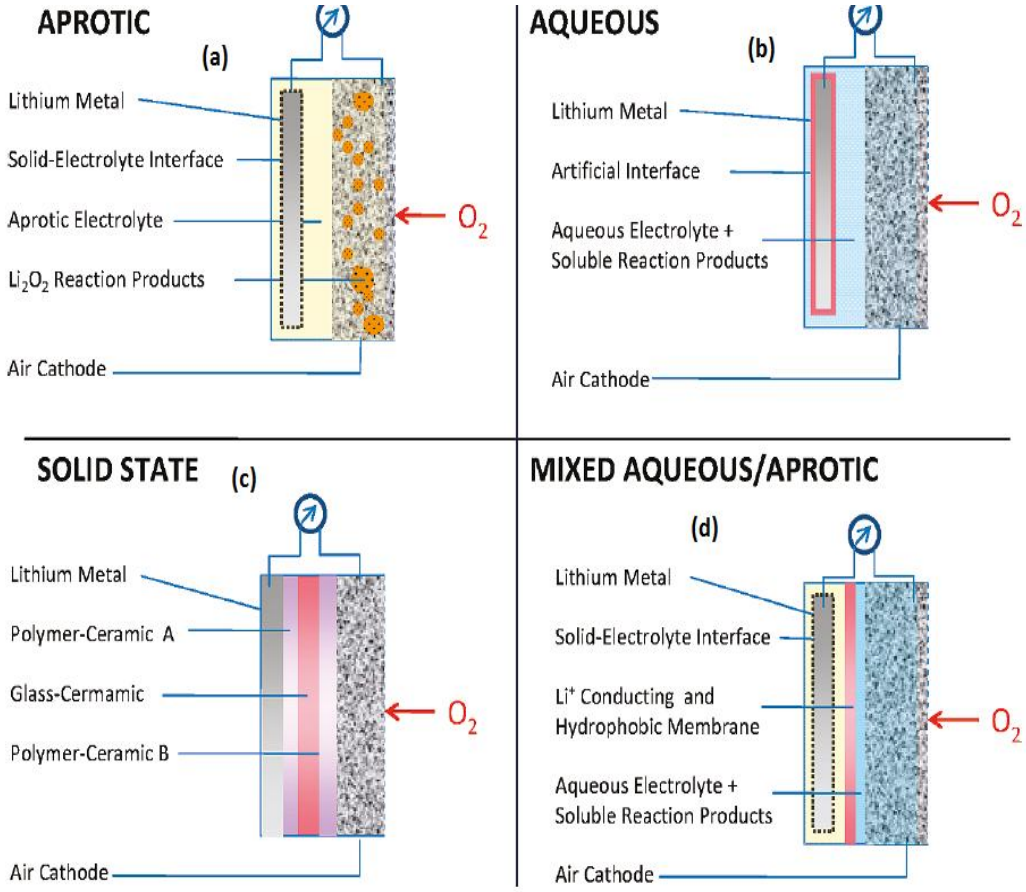

Figure 1: Four different architectures of Li-air batteries in which Li metal is used as anode material. Aprotic, aqueous, mixed aprotic/aqueous are liquid electrolyte based architecture (4).

The architecture of aqueous Li-air cell is shown schematically in (Figure 1b). Metallic lithium is used as anode covered with Li-ion conducting ceramic film, which prevents vigorous reaction of metallic lithium with water. The aqueous electrolyte consists of lithium salts dissolved in water. Catalyst is needed with positive electrode that reduce activation energy barrier for the oxygen reduction reaction (ORR) and the oxygen evolution reaction (OER). The main advantage is that discharge reaction product is soluble in water. The disadvantage is that energy density of aqueous system is much lower than that of conventional Li-ion batteries because of narrow electrochemical window of water (3).

Solid-state Li-air batteries composed of lithium metal as anode, glass-ceramic electrolyte, and a porous carbon cathode (Figure 1c). The anode and cathode are separated from the solid electrolyte by the polymer ceramic membrane. The polymer ceramic composites are

used to reduce overall impedance. For example ,18.5Li_2O6.07$Al_2O_3$37.05$GeO_2$37.05P_2O_5, LAGP and two layers of polymer (ethylene oxide) (PEO) incorporated with Li-salt LiN $(SO_2CF_2CF_3)_2$ (LiBETI). Advantage of Solid state Li-air battery system is LAGP could completely prevents the reaction of H_2O or CO_2 with the negative Li electrode. However, the main drawback is its low conductivity (5).

Metallic lithium is used as anode in mixed aqueous/aprotic Li-air battery system (Figure 1d). One part of the electrolyte is aqueous and another part is aprotic. The porous cathode is in contact with aqueous electrolyte and the Li-metal anode with non-aqueous electrolyte. Two electrolytes are separated with a lithium conducting ceramic (5).

1.2.2 Lithium ion batteries

Lithium ion batteries are rechargeable batteries in which Li-ion moves from anode to cathode during discharging and back to anode during charging process. Intercalated lithium compounds are usually used as electrode materials. In lithium-ion batteries aqueous electrolyte, organic electrolyte or composite electrolyte can be used. Due to high reactivity to water non-aqueous or aprotic solvent are preferred. Non-aqueous electrolytes consist of Li-salts e.g., $LiPF_6$, $LiBF_4$ or $LiClO_4$ in organic solvent (ethylene carbonate, dimethyl carbonate, and diethyl carbonate).Organic solvent decomposes during charging and form solid electrolyte inter phase (SEI). Room temperature ionic liquids are alternative solvents to limit the flammability and volatility of aprotic solvents. In Li-ion batteries, various lithium compounds such as lithium cobalt oxide ($LiCoO_2$), Lithium iron phosphate (LFP), lithium manganese oxide (LMO), lithium nickel manganese cobalt oxide (NMC), Lithium nickel cobalt aluminum oxide (NCA) and lithium titanate (LTO) etc are used as anode materials (6). Electrochemical reaction of cobalt based Li-ion batteries is given in table 1.

1.2.3 Metal air Batteries

Metal air batteries (lithium-air, iron-air, aluminum–air, magnesium-air and zinc–air) have recently attracted much attention due to their high energy density. Cathode of metal air battery utilizes oxygen from air (ambient) and air act as reactant in the electrochemical reaction. Recently, it has been shown that theoretically it is possible that Li-air battery can

have specific energy of 11,680 Wh/Kg, which is close to gasoline (figure 2). Suggested cell reaction and theoretical energy density, practical energy density of different batteries are given in table 1. Littauer and Tsai (7) in 1976 introduced the concept of Li–air chemistry. Abraham in 1996 presented non-aqueous Li-O_2 battery and Bruce discovered the reversibility of the system in 2006. Their work attracted great attention and triggered numerous research projects on this system.

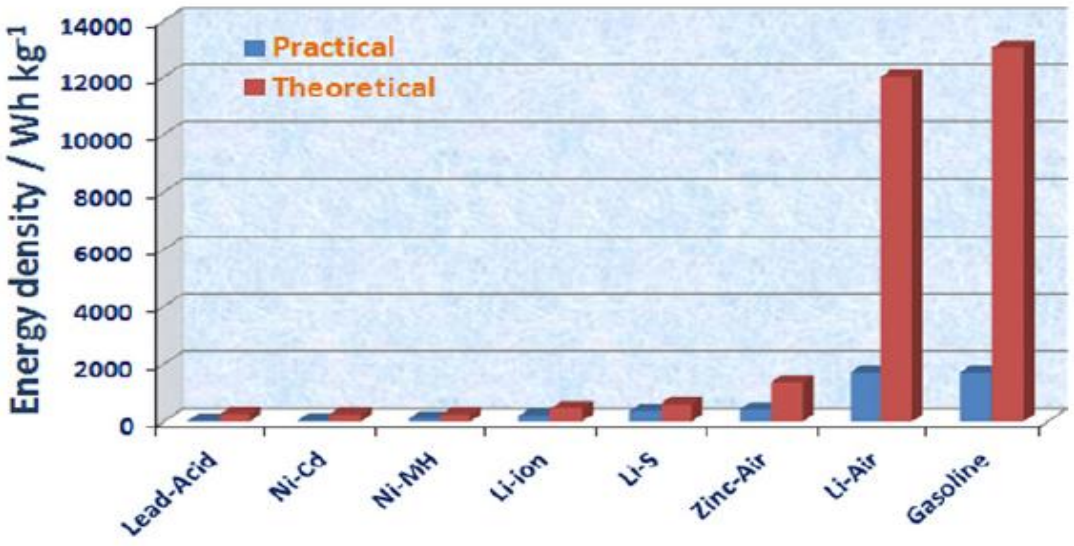

Figure 2: The gravimetric energy densities (Wh/kg) for various types of rechargeable batteries compared to gasoline (7).

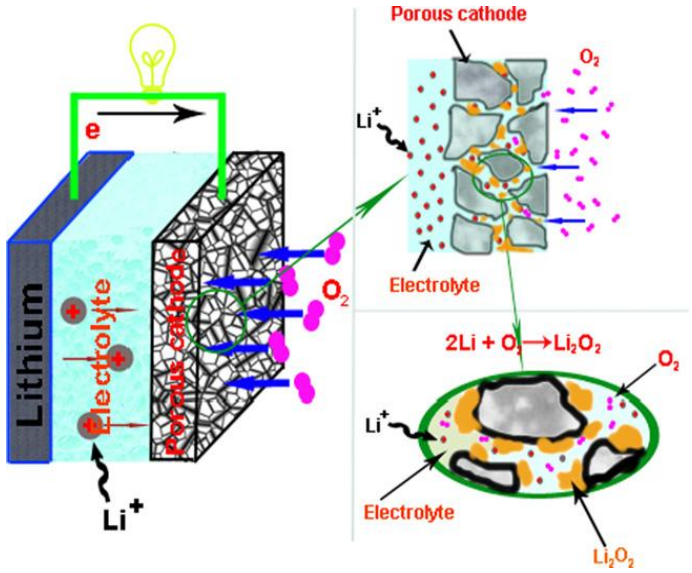

Figure 3: The schematic figure of a non-aqueous Li–air battery and the porous cathode structure (7).

Li–air battery is a key research area for next-generation power sources which would ideally can turn the entire vehicle into electric to reduce emission to the environment. At present practical energy density of Li-air battery is far from its theoretical energy density. In order to improve the Li-air battery, we need to understand its reaction mechanisms.

A schematic diagram of non-aqueous Li-air battery system is given in figure 3. Where oxidation reaction occurs at the anode and electron flow through external circuit and Li^+ ion react with oxygen and form Li_2O_2 in the cathode. During charging Li_2O_2 decomposed to Li^+ and oxygen.

Table 1: Electrochemical reactions and energy densities of the various rechargeable batteries **(8).**

Types	**Cell reactions**	**Theoretical energy density (Wh/Kg)**	**Practical energy density (Wh/Kg)**
Lead–Acid	**$Pd + PdO_2 + 2HSO_4^- + 2H^+ \rightarrow 2PdSO_4 + 2H_2O$**	**170**	**30–50**
Ni–Cd	**$2NiO(OH) + Cd + 2H_2O \rightarrow 2Ni(OH)_2 + Cd(OH)_2$**	**245**	**45–80**
Ni–MH	**$xNi(OH)_2 + M \rightarrow xNiOOH + MHx$**	**280**	**60–120**
Li-ion	**$LiCoO_2 + C \rightarrow LixC + Li1-xCoO_2$**	**400**	**110–160**
Li–S	**$xLi^+ + S8 + e \rightarrow Li_2Sx$**	**2600**	**~400**
	$Li_2Sx + Li^+ + e \rightarrow Li_2S_2$ or Li_2S		
Zn–air	**$2Zn + O_2 \rightarrow 2ZnO$**	**1084**	**~400**
Li–air	**$2Li + O_2 \rightarrow Li_2O_2$**	**11,680**	**~2000**

1.2.4 Drawbacks of air cathodes-electrolyte

Understanding the mechanisms of the ORR in non-aqueous solutions is the main key to develop high efficiency and power capability of Li-air battery (9). Li-metal which is high capacity electrode contains the ionic charge carriers. Li metal reacts with electrolyte and leads to formation of unstable decomposition layer. When Li metal is immersed in an organic solvent, it spontaneously reacts to form Li-ion conducting film on its surface. The reaction between lithium and solvent takes place and a multi layer deposition of Li-salt creates mass diffusion barrier which inhibits the reaction kinetics (4). The air cathode provides an interface where O_2 from the air is reduced on the surface of the cathode. Carbon with or

without catalyst enhances the rate of O_2 reduction. The product of the discharge in the Li-air cell is Li_2O and Li_2O_2 which are not soluble in organic electrolyte solutions (10).

Finding a suitable and stable electrolyte for a Li–air battery is a major challenge as well as cost effective catalysts to reduce over-potentials for the discharge and charge reactions. Development of nanostructured air cathode materials can optimize transport of all reactants to active surface of the cathode and provide sufficient space for discharge product. In order to supply contaminants free O_2 to the system a high throughput air breathing membrane which can separate O_2 from air and can avoid H_2O, CO_2 and other contaminants needs to be developed (4). To achieve high energy density, a high positive electrode capacity needs to be developed for Li-air cell. The major capacity limiting factors are passivation, pore blockage, and O_2 transport limitations. Passivation of electrode surface by electronically insulating discharge products limit the Li-air battery capacity as low discharge rate. Blockage of micro pore cathode by Li oxides and other byproducts can limit accessibility of electrode surface for electrochemical reaction (3).

Another problem associated with air cathode electrode in non-aqueous electrolyte is the deposition of insoluble reaction product Li_2O_2 at active sites. Once a dense product layer is formed on the entire active surface, ionic or electronic transport become limited through the product layer. Due to poor electronic conductivity of the product Li_2O_2, the discharge current density decreases with the increase in the thickness of the product layer, which eventually leads to the termination of electrode reaction. Another problem is linked with Li–air battery is that the use of catalysts in electrode surface to enhance the electrode kinetics and reduce the energy loss associated with the discharge–charge polarization. Proper distribution and loading influence the cathode reaction as well as performance of the Li–air battery. Oxygen transport is another challenge for Li-air battery research. Sufficient porosity and minimal tortuousness is needed for proper oxygen transport to the active sites of electrode with minimum energy loss. The resistance to the transport of O_2 and Li-ions through the pores decrease and electron transport (11).

Nano structured electrodes are used for Li-air battery to get better performance but due to complex synthesis process fabrication cost becomes high. Nano structured electrodes have

large surface area which allows to have undesired side reactions between the electrode and electrolyte (11).

Layered cathode can be operated at high voltages and have exhibited high capacities (12). One example spinel $LiMn_{1.5}Ni_{0.5}O_4$, olivine $LiCoPO_4$, and olivine $LiNiPO_4$ which can be operated at high voltage and showed high capacity. However, the major difficulty is that these cathodes are unstable in organic electrolytes. Like $LiPF_6$ in 1:1 ethylene carbonate (EC)/diethyl carbonate (DEC) electrolyte form an SEI layer on the cathode surface during discharge which becomes severe and aggressive at elevated temperatures ($\sim 55^0$C) after subsequent cycles. These reactions degrade the electrolyte and cathode, which results in the capacity failure. Reactivity of highly oxidizing cathode surface could also be problem also for long term stability and life cycle of electrolyte (12).

Olivine $LiFePO_4$ (1-d structure) used as cathode showed low electronic and Li^+ ion conductivity. Small particle size and carbon coating is needed to realize high rate capability, which results in high processing cost. If layered $LiCoO_2$ cathode (2-d structure) used as cathode, only 50% of the theoretical capacity can be utilized due to safety concern (12).

Another problem is that porous carbon is flooded while contacting with non-aqueous electrolyte and discharge product (Li_2O_2, Li_2O) insoluble in electrolyte are precipitated into cathode pores and this restricts the transport of oxygen towards the pores where reaction takes place. Electrolyte's ability to properly transport the oxygen depends on electrolyte parameters such as oxygen solubility and oxygen diffusion (13).

Solvent plays an important role in determining cycling characteristics and efficiency of the rechargeable Li-air battery. Recent studies revealed that organic carbonates, esters and ethers are not good candidates as electrolytes for Li-air battery due to decomposition during discharging and Lithium carbonate ($LiCO_3$) and lithium alkyl carbonate (RO-(C=O)-OLi) were identified after few cycles. The reason for carbonate species generation is chemical reaction between Li_2O_2 and carbonate base electrolyte. Research proved that Li_2O_2 is highly reactive against carbonate solvents, moisture and CO_2 gas (1). However, esters and ethers based electrolytes are relatively more stable than organic carbonates (14), (15), (16). The dominant decomposition pathway was found in the O-alkyl carbon atom of organic carbonates where super oxides attack nucleophilically. Computational studies have revealed that lithium

superoxide, also lithium peroxide itself can act as degradation agent for carbonate and esters based solvents. For example, it has been shown that in the presence of lithium peroxide, propylene carbonate (PC) is irreversibly decomposed (17). The main drawback regarding carbonate based organic electrolytes is that the attack of the solvent molecule by superoxide radical anion. XRD results of the discharge air electrodes showed that lithium propylenedicarbonate (LPDC), or lithium ethylenedicarbonate (LEDC) and lithium carbonate (Li_2CO_3) are constantly the main discharge products rather than lithium peroxide (Li_2O_2) or lithium oxide (Li_2O). In situ GC-MS analysis indicates that Li_2CO_3 and Li_2O can't be oxidize at potential as high as 4.6V vs. Li/Li^+. However, other discharge products are readily oxidized .The superoxide attack on the solvent molecules at faster rate so that the formation of LiO_2 from superoxide radical anion and the Li-ion is slower than super oxide attack, results solvent degradation (18).

1.2.5 Progress regarding Li-air cathode

Recent studies have been considering ethers and glymes as solvents for Li-air batteries because these are more stable than organic carbonates against nucleophilic attack by superoxide. However, for long term cycling of rechargeable Li-O_2 battery ethers and glymes are unstable (19).

1:1 (EC:PC) with lithium salt, LiTFSI showed higher discharge capacity than all the electrolytes containing ethers and glymes. The PC–DME based electrolytes have even high capacity and oxygen solubility than PC-EC. TPFPB is a good additive which can partially dissolve Li_2O and Li_2O_2 and oxygen solubility also increases when TPFPB added (20).

Most recent study revealed that ionic liquid N-methyl-N-propylpiperidinium bis (trifluoromethansulfonyl) amide (PP13TFSA) is an appropriate candidate as a solvent. Quantitative analysis was carried out by gas chromatography to measure the amount of evolved gases from different organic electrolytes, which are listed in table 2.

Table 2: Compositions and their normalized concentration of various gases stored during the initial charge by gas chromatography. Amounts of the evolved gases were normalized by the electrical quantity during charging (21).

Electrolyte solvent	**Classification**	**Norm. gas conc. [L/Ah]**		
		H_2	**CO**	**CO_2**
PP13TFSA	**–**	**0.311**	**0.000**	**0.000**
EC-DEC	**Carbonate**	**0.114**	**0.028**	**0.555**
PC	**Carbonate**	**0.035**	**0.014**	**0.676**
GBL	**Lactone**	**0.579**	**0.079**	**0.826**
TEGDME	**Ether**	**0.197**	**0.007**	**0.001**

Studies on the use of catalysts have revealed that over potential of charging process can be reduced. MnO_2 is the best studied metal oxide, which is used as catalyst to promote oxidation of Li_2O_2. However, its efficiency as catalyst depends on the structure and morphology. Among the different metal catalysts the manganese-catalyzed air cathodes have shown the highest specific energy about 4000mAh/g. Another study found that Au/carbon cathode promotes the ORR process and Pt/carbon cathode promotes the OER process. But metals Au, Pt are economically unfeasible (22). By using CeO_2 as catalyst a smooth increase in the ORR rate and reduction in the polarization was seen. Capacity of 2128mAhg^{-1} displayed when CeO_2 was used as catalyst. Not only surface area but also crystal structure plays important role on the elctrocatalytical performance of different catalysts in the Li-air batteries (23).

Recent studies have revealed that the presence of redox mediator with a lower potential in the electrolyte of the rechargeable non-aqueous Li-O_2 battery could recharge at higher current density (1 mA/cm^2). The tetrathiafulvalene (TTF) molecule is oxidized to TTF^+ at the cathode surface which in turn oxidizes the insulating solid (Li_2O_2) and TTF^+ reduces back to TTF. Effective oxidation of Li_2O_2 leads to complete reversibility of Li air battery. Here, this mediator act as an electron hole transfer agent that permits effective oxidation of Li_2O_2. However, the absence of redox mediator leads to severe polarization on charging (24).

Chapter 2

2 General theory of electrochemistry

Electrochemistry is the branch of chemistry which deals with the interrelation of electrical and chemical effects. A large part of this field deals with the study of chemical changes caused by the passage of an electric current and the production of electrical energy by chemical reactions. In Electrochemistry electron transfer reactions take place at the solid solution interface. The solid is the electron conductor i.e., the electrode and ionic conductor is the electrolyte. In this section most relevant and important equations and theory will be discussed (25).

2.1 Oxidation-reduction potentials

Oxidation and reduction involves the transfer of electron between substances. Both processes take place simultaneously. If one substance loose electron, another substance gain that electron. Equilibrium potential of redox reactions are directly related to thermodynamics and also specify at which potentials reduction and oxidation reaction take place in the absence of kinetic limitations. This potential depends on pH and can be measured as relative to a reference electrode placed in the solution.

2.2 Mass transport

There are three kinds of mass transport processes such as diffusion, convection and migration, which can influence electrochemical reactions. Diffusion occurs in solution when relative concentration of a reagent is dense. Diffusion can be defined as movement of species under the influence of chemical potential gradient (i.e concentration gradient). Action of force on solution generates convection. This action can be pump, a flow of gas or even gravity. Fluid flow occurs because of natural convection. It is caused by density gradient. Force convection can be characterized by stagnant regions, laminar flow and turbulent flow. Final form of mass transport is considered as migration. Migration caused due to a gradient of electrical potential (26).

2.3 Essential electrode Reaction

An electrode reaction can be characterized by the Nernst equation. The Nernst equation illustrates the relation between the concentration of the redox species at the electrode surface and applied potential on electrode. In general case O is capable of being reduced to R at the electrode by the following reversible electrochemical reaction.

$$O + ne \leftrightarrow R$$

$$E = E^{0\prime} + \frac{RT}{nF}\, ln \frac{C_0^*}{C_R^*} \qquad \textbf{Eq1}$$

Where C^*_R and C^*_0 are the bulk concentrations of reduced and oxidized species respectively, and E° is the formal potential.

If the system follows the Nernst equation the electrode reaction is often said to be thermodynamically or electrochemically reversible. A process can either reversible or not depends on time dependent measurements, the rate of change of driving force and a speed at which the system can establish equilibrium. A given system can behave reversibly in one experiment and irreversibly in another under different experimental conditions (25).

2.4 Heterogeneous rate constant

Redox reactions in non-aqueous solvent involved electron transfer (ET) process. Solvent has remarkable influence on the ET process that occurs either homogenously in the solution or heterogeneously at the electrode surface. The rate constant of ET process which occurs heterogeneously is called heterogeneous rate constant. ET rate constant is proportional to the exponential of the applied voltage. Simple electrochemical methods such as CV, RDE can be used to determine rate constant of an ET process (27).

2.5 Cyclic Voltammetry

Cyclic voltammetry is one of the most versatile and commonly used techniques for studying the electrochemical reactions. In the cyclic voltammetry (CV) potential on the working electrode is scanned linearly backward and forward within the pre defined limit. The

resulting current on the working electrode is measured as function of the applied potential. Figure 4 shows potential input in cyclic voltammetry (25). CV can be used for different purposes. For example, it can be used to acquire qualitative information about electrochemical reaction but also quantitative information about reaction kinetics and mass transport. From cyclic voltammetry the type of reaction and rate of reaction can be determined by using some equations such as the Randles-Sevcik equation, Nicholson and Shain equation 25).

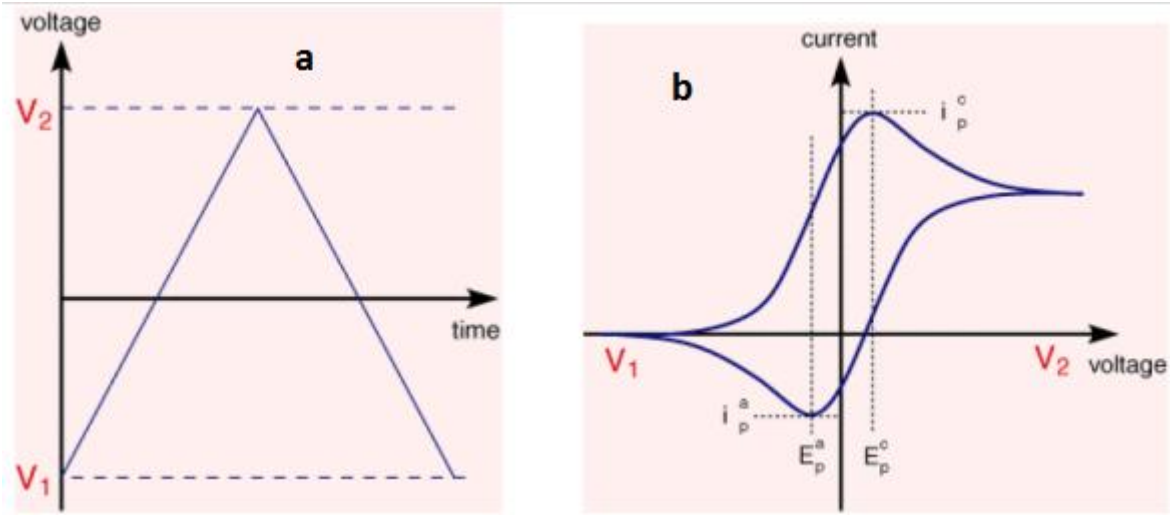

Figure 4: (a) Potential as a function of time and (b) current as a function of voltage for cyclic voltammetry (25).

2.5.1 Scan rates

Dependence of the oxidation/reduction peak potentials on scan rate is good indicator if an electrochemical reaction is reversible, quasi-reversible or irreversible. For reversible reactions, the oxidation and reduction peak potentials do not change with scan direction, for Quasi or irreversible reactions peak potentials shift in the scan direction (figure 5). Current density also depends upon the scan rate and increases at high scan rate because the concentration of electroactive species increases in diffusion layer. Reversible electrochemical reactions has some characteristics such as, peak position do not change with scan rate, ratio of oxidation and reduction peak current should be one and peak current is proportional to square root of the scan rate (25).

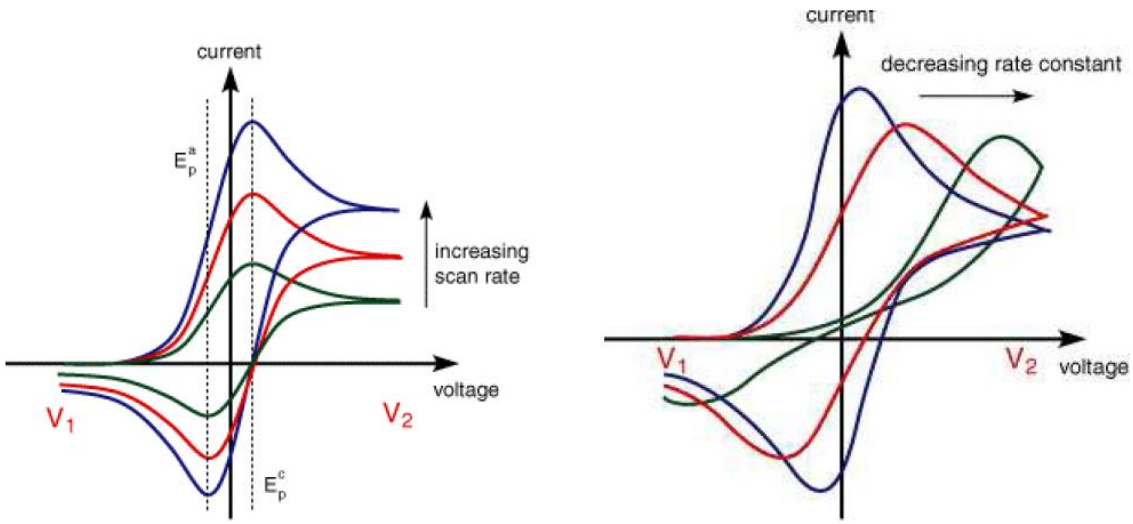

Figure 5: Scan rate and rate constant dependence of cyclic voltammetry curve

2.5.2 Reversible systems

A theoretical expression of peak current for a reversible cyclic voltammogram is derived as a function of the scan rate which is called Randles-Sevcik expression. According to this expression, the dependence of peak current I_p on scan rate v can be written as shown below,

$$i_p = 2.69 \times 10^5 n^{3/2} A D^{1/2} C v^{1/2} \qquad \text{Eq2}$$

Where, i_p= peak current, A

n= electron stoichiometry

A= electrode area, cm^2

D= diffusion coefficient, cm^2s^{-1}

C= concentration, $molcm^{-3}$

v= scan rate, Vs^{-1}

i_p increases with $v^{1/2}$ and is directly proportional to concentration. This expression is very important in the study of electrochemical mechanisms. The ratio of anodic and cathodic peak currents should be close to one.

For a reversible electrochemical reaction, the number of electron transferred in the electrode reaction can be determined by the anodic and cathodic peak potentials

$$\Delta E_p = \frac{E_{pa} - E_{pc}}{n} \cong 0.059 \qquad \textbf{Eq 3}$$

Where ΔE_p is potential separation, E_{pa} is anodic peak potential and E_{pc} is cathodic peak potential (25).

2.5.3 Irreversible and Quasi-Reversible Systems

For irreversible system individual oxidation and reduction peaks are reduced in size and separated widely. Totally irreversible systems are characterized by shift of peak potential with the scan rate:

$$E_p = E^{0'} - \frac{RT}{\alpha F}\left[0.780 + \ln\left(\frac{D_0^{\frac{1}{2}}}{k^0}\right) + \ln\left(\frac{\alpha F v}{RT}\right)^{1/2}\right] \qquad \textbf{Eq 4}$$

$$\vdots E_p - E_{p/2} \vdots = \frac{1.857RT}{\alpha F} = \frac{47.7}{\alpha}\ mV \quad \text{at } 25^0\text{C} \qquad \textbf{Eq 5}$$

Where α is the transfer coefficient, and n is the number of electrons involved in the charge transfer step, R is the gas constant, F is Faraday constant, T is temperature. The potential E_p occurs at a higher value than E_0 with the over potential related to k_0 and α.

Charge transfer coefficient is a measure of the symmetry of the energy barrier. Charge transfer coefficient is independent of any mechanistic reflection and based on experimental data and is used for the elucidation of electrode kinetics.

Nicholson and Shain equation is usually used to analyze Irreversible and Quasi-Reversible systems. According to Nicholson and Shain, peak current is given by,

$$I_p = 2.99\times10^6 n\,(n\alpha)^{1/2} A C D^{1/2} v^{1/2} \qquad \textbf{Eq 6}$$

Where area is A, concentration C, diffusion coefficient is D, α charge transfer coefficient
Here peak current is still proportional to bulk concentration.
For quasi-irreversible systems the current is controlled by mass transfer and charge transfer. The standard heterogeneous rate constant range for quasi-irreversible systems is: $10^{-1} > k_o > 10^{-5}$ cm/s. Peak separation is quite larger than reversible system. The expression which is used to calculate rate constant of quasi-irreversible systems,

$$\Psi = \Delta\pi^{-1/2} = \frac{(\frac{D_0}{D_R})^{\alpha/2} k^0}{(\pi D_0 f v)^{1/2}} \qquad \textbf{Eq 7}$$

Where Ψ equivalent parameter, D_0 is oxidation diffusion coefficient, D_R is reduction diffusion coefficient, Faraday constant F, scan rate v (28).

2.6 Uncompensated Resistance

If potential profile is considered in solution between the working and auxiliary electrodes, the solution between these electrodes can be regarded as potentiometer. Uncompensated resistance can affect the measured value of current or potential. It is denoted by R_u .It also depends on the electrode size. This can be minimized by the use of three electrode system.

2.7 Rotating Disk Electrode (RDE)

RDE is one of the most popular hydro dynamic methods used in a three electrode system. The electrolytes are forced by convection to a rotating disk electrode. When the rotating speed increases the species flux to the surface increases by convection and current also increases. The rotating disk electrode (RDE) is one of the few convective electrode systems where hydrodynamic equations and the convective equations have been solved rigorously. This technique is very simple to construct and consists of a disk of the electrode material inserted in a rod of an insulating material.

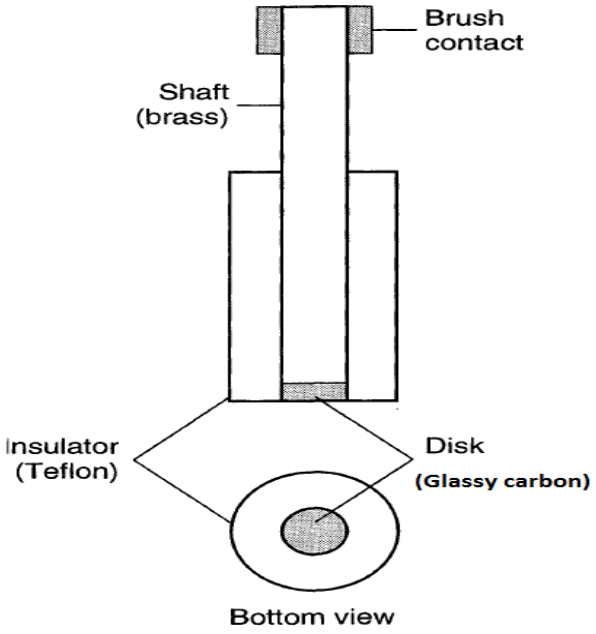

Figure 6: Schematic view of Rotating disk electrode.

A schematic view of RDE is given in figure 6. At stationary electrodes the diffusion layer can grow independently. By using convective methods such as RDE, the growth of diffusion layer can be restricted. The role of mass transport on electrode reaction kinetics can be elucidated from the kinetic parameters obtained from CV and RDE experiments (25).

Dr. Benjamin Levich illustrated first the mathematical treatment of convection and diffusion for rotating disk electrode,

$$I_L = 0.62nFAD_0^{2/3}\omega^{1/2}\nu^{-1/6}C_0^* \qquad \textbf{Eq8}$$

I_L is the current limited in voltammogram

n is the number of electrons transferred,

F is the Faraday constant

A is the electrode area

D_0 is the diffusion coefficient

ω is rotation speed

v is the kinematic viscosity of the solution and

C_0 is the concentration of the electroactive species

This equation only applies to the mass transfer limited condition at RDE and assumes I_L is proportional to C_0^* and $\omega^{1/2}$. $\frac{I_L}{\omega^{1/2}C_0^*}$ is also called levich constant.

For totally irreversible one step one electron reaction is analyzed by the Koutecky-Levich equation which is given below,

$$\frac{1}{i} = \frac{1}{i_K} + \frac{1}{i_L} = \frac{1}{i_K} + \frac{1}{0.62nFAD_0^{2/3}\omega^{1/2}\nu^{-1/6}C_0^*} \quad \textbf{Eq9}$$

Where i_K represents the current in the absence of any mass-transfer effects, i_L is the current limited in voltammogram, n is the number of electrons transferred and F is the Faraday constant, A is the electrode area, D_0 is the diffusion coefficient, ω is rotation speed, ϑ is the kinematic viscosity of the solution and C_0 is the concentration of the electroactive species. $\frac{i}{\omega^{1/2}C}$ is a constant only when i_K is very large (28).

Studies showed that the current is often exponential to the over potential η, that is given by Tafel in 1905,

$$\boldsymbol{\eta = a + blogi_0} \quad \textbf{Eq 10}$$

It is a successful model of electrode kinetics, known as Tafel equation where $\boldsymbol{a = \frac{2{,}3RT}{\alpha F}logi_0}$ and $\boldsymbol{b = \frac{-2{,}3RT}{\alpha F}}$ **Eq11**

Where I_0 is exchange current which can be considered as idle current. A plot of Log I_k (kinetic current) vs η (over potential) known as Tafel plot, is a useful technique for estimating kinetic parameters. A schematic diagram of tafel plot is given bellow,

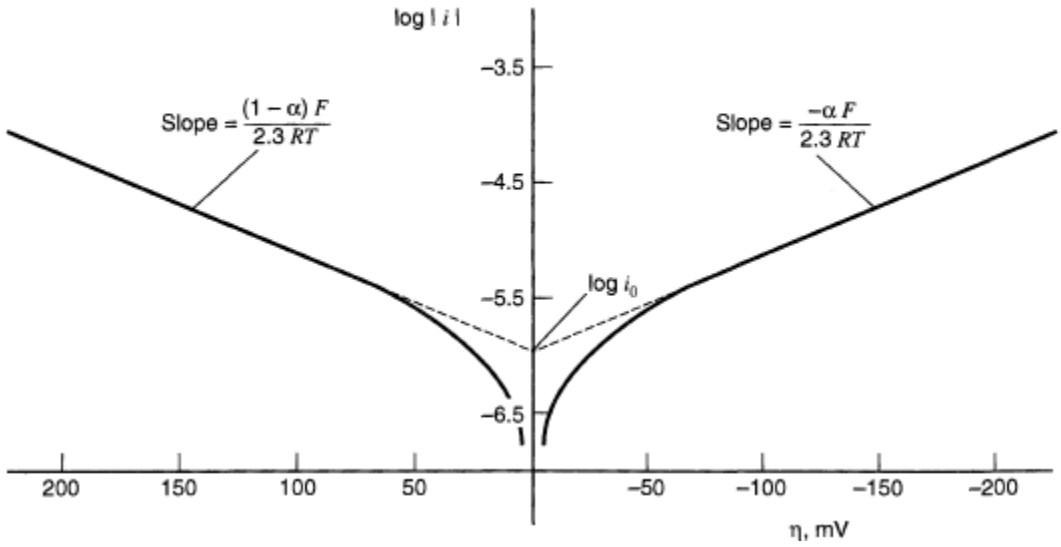

Figure 7: Tafel plots for anodic and cathodic branches of the current over potential curve.

A Tafel relationship cannot be observed for the systems where the mass-transfer effects on the current are absent. At these points Tafel behavior is an indicator of totally irreversible kinetics. Tafel slope can also be used to determine either the reaction is reversible or not. For one electron reversible reaction slope of Tafel plot should be 120mV/dec. (25).

Chapter 3

3 Experimental

The main focus of the project is to utilize electrochemical methods for analyzing reaction mechanism. Here overview of setup, experimental procedure and electrochemical techniques are described.

3.1 Materials

Dimethyl Sulfoxide (DMSO)(Anhydrous,99,9%), acetonitrile (MeCN)Anhydrous,99,9%, tetrabutylammonium hexafluorophosphate ($TBAPF_6$) (electrochemical grade, ≥99, 0%), lithium hexafluorophosphate ($LiPF_6$) (battery grade, >99,9%), Lithium perchlorate ($LiClO_4$) (battery grade, dry 99, 99%) were purchased from Sigma Aldrich. All chemicals were immediately stored in glove box filled with purified argon where the moisture and oxygen content was less than 1ppm.Medium size glove bag was purchased from Sigma Aldrich.

3.2 Potentiostats

Potentiostats used in these experiments are as follows,

- Gamry Reference 600^{TM} , Gamry Analyst 5.6 Potentiostats/Galvanostat and
- Atutolab, NOVA 1.8

3.3 Cells and electrode setup

For all experiments three electrode cell system was used (figure 5). Glassy carbon was used as working electrode (dia-5mm), pt mesh was used as counter electrode and Ag/AgCl, Ag/Ag+ was used as reference electrode. The Ag/AgCl electrode was prepared by oxidation of Ag wire in saturated KCl in H_2O. The Ag/Ag+ electrode was prepared by oxidation of Ag wire in 0.001M $AgNO_3$/MeCN and outer junction was filled with working solution (MeCN or DMSO). The surface area of counter electrode was much larger than working electrode to restrict the limitations of the processes occurring at the working electrode.

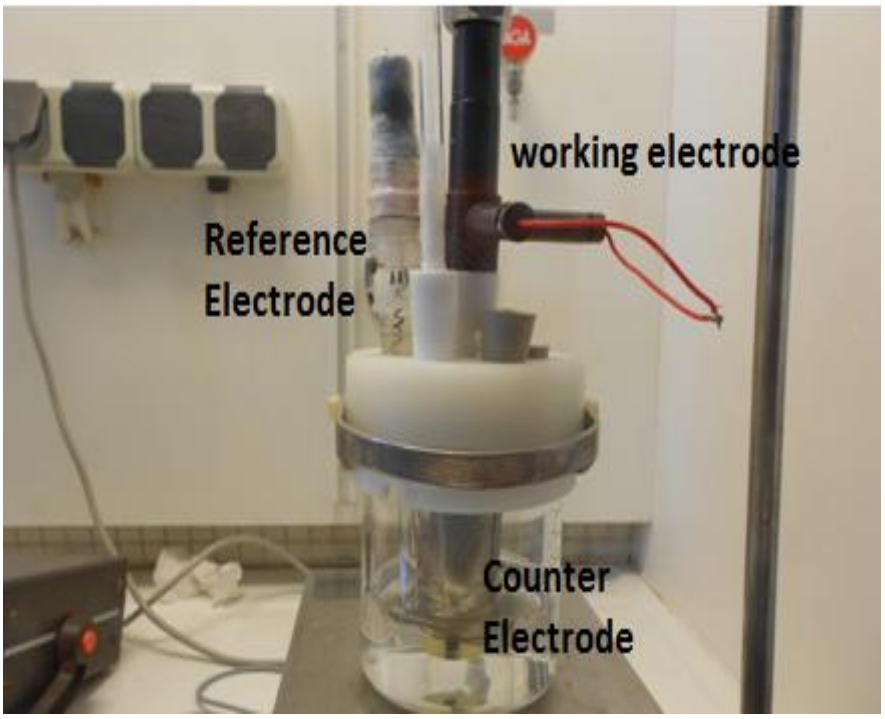

Figure 8: Schematic setup of three electrode system used in all experiments.

3.4 Measurements Procedure

All solution preparations were carried out inside of glove box filled with dry Argon, where the moisture and oxygen content was less than 1ppm.Measured salt and solvent were mixed by a stirrer at 600rpm. Experiments were carried out inside the glove bag filled with dry Argon. Before start of the experiments the glove bag was evacuated two times in order to remove moisture and air from the glove bag.

3.5 Electrochemical Experiments

The electrochemical experiments were performed with two different setup, Gamry Reference 600^{TM}, Gamry Analyst 5.6 potentiostats/Galvanostat and an Autolab (Ecochemie Inc., model-PGSTAT 12) equipped with electrochemical cell. The electrochemical cell was built in house consisted of traditional three electrode system utilizing Ag/Ag reference electrode. The cell had inlet and outlet valves for oxygen or argon purging. The glassy carbon of 5mm diameter used as working electrode was polished with 0,3µm alumina paste and rinsed thoroughly with milli-Q water and dried carefully prior to the experiments. All the

cyclic voltammetry was performed in argon filled glove bag (atomsbag two-hand non-ster, slide closer, size M 39''×48'', sigma-aldrich) where H_2O and O_2 concentration were kept bellow 1ppm at room temperature. For RDE experiments glassy carbon electrode was rotated with RDE rotor. For the ORR measurement the solution were purged with pure $O_{2.}$ The effect of sweep rate on the voltammograms were observed by using same concentration of electrolyte at different scan rates 25, 50, 100, 200, 300, 400, 500 mVs^{-1}. Initial condition was set as step size 2mV, equilibrium time 5 s and I/R range was kept fixed for all CV scan. Different potentials range (±V) was chosen for each scan. Open circuit potential and impedance of each electrolyte was measured. For impedance measurements, the spectra were measured in the frequency range from 1Hz to 100000 Hz at an open circuit potential. For all RDE measurements I/R range was kept as auto module. Rotation speed of 300,750, 1000, 1250, 1700, 2000, 2500, 3000, 3550, 4000, 5000 RPM used for the RDE experiments.

Chapter 4

4 Results and discussion

Non-aqueous solvents are best media for investigating the oxygen reduction reactions (ORR) relevant for the Li-air battery system. Literature studies revealed that three possible O_2 reduction products such as LiO_2, Li_2O_2, Li_2O are formed and these are highly polar. In order to dissolve these products and avoid their passivation of electrode surface, polar solvents are required. There are several aprotic solvents which were studied for Li-air battery research. In the study dimethyl sulfoxide (DMSO) and acetonitrile (MeCN) were chosen to investigate the fundamental reaction mechanisms of Li-air battery. Three different salts i.e., $LiPF_6$, $LiClO_4$ and $TBAPF_6$ were chosen for this study. The properties of DMSO and MeCN are given in Table 3.

Table 3: Chemical and physical properties of solvents (29).

Solvent	Dielectric constant (25^0C)	Donor Numbers (kcal/mol)	viscosity η (cP)	oxygen solubility (mM/cm^3)
DMSO	48	29.8	1.948	2.1
MeCN	36.64	14.1	0.361	8.1

4.1 Oxygen Reduction in 0.1M $TBAPF_6$/DMSO

The role of $TBAPF_6$ on the reduction properties of oxygen in DMSO were studied by using cyclic voltammetry (CV) and rotating disk electrode (RDE) voltammetry. Glassy carbon was used as working electrode, because real cathode materials are also made of carbon. Figure 9 displays cyclic voltammetry (CV) for the reduction of oxygen in a 0.1M $TBAPF_6$/DMSO electrolyte. The reference electrode which was used in the CV experiments was Ag/Ag+. Peak potentials separation between anodic (Epa= -1.19V) and cathodic (Epc= -1.125V) is 65mV, which is close to 60mV. Peak current ratio is close to unity. These results indicate that O_2 reduction in the presence of TBA^+ ions is reversible.

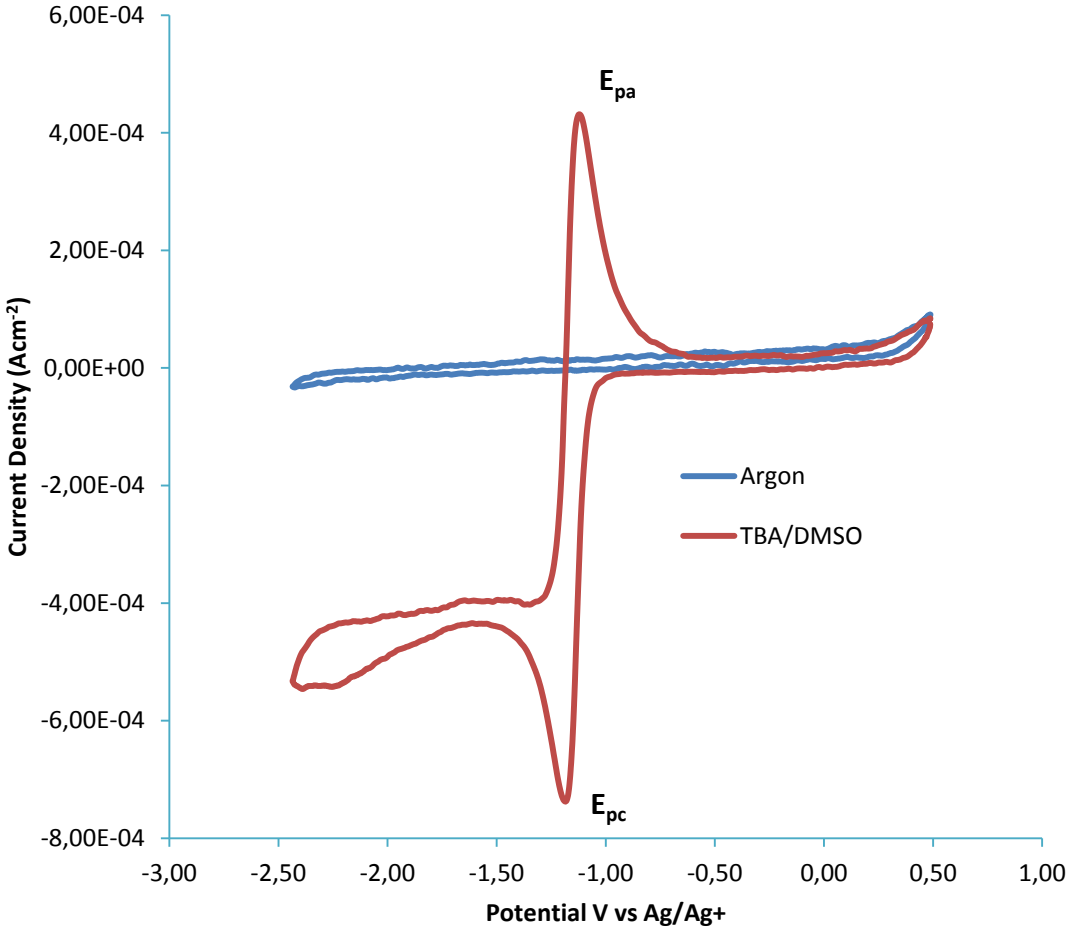

Figure 9: Cyclic voltammograms for the reduction of oxygen in 0.1M $TBAPF_6$/DMSO on a glassy carbon working electrode at a scan rate of $100mVs^{-1}$.The values are IR corrected. The blue curve is argon background.

In Figure 10 cyclic voltammograms for the reduction of oxygen-saturated $TBAPF_6$/DMSO at different scan rates (50mV to 400mV) are shown. Reduction seems to be reversible at all sweep rates. However there is slight shift in peak position. The Randles-Sevcik plots presented in Figure 11 by using equation 2 are linear, which indicates a fast diffusion controlled electrochemical process.

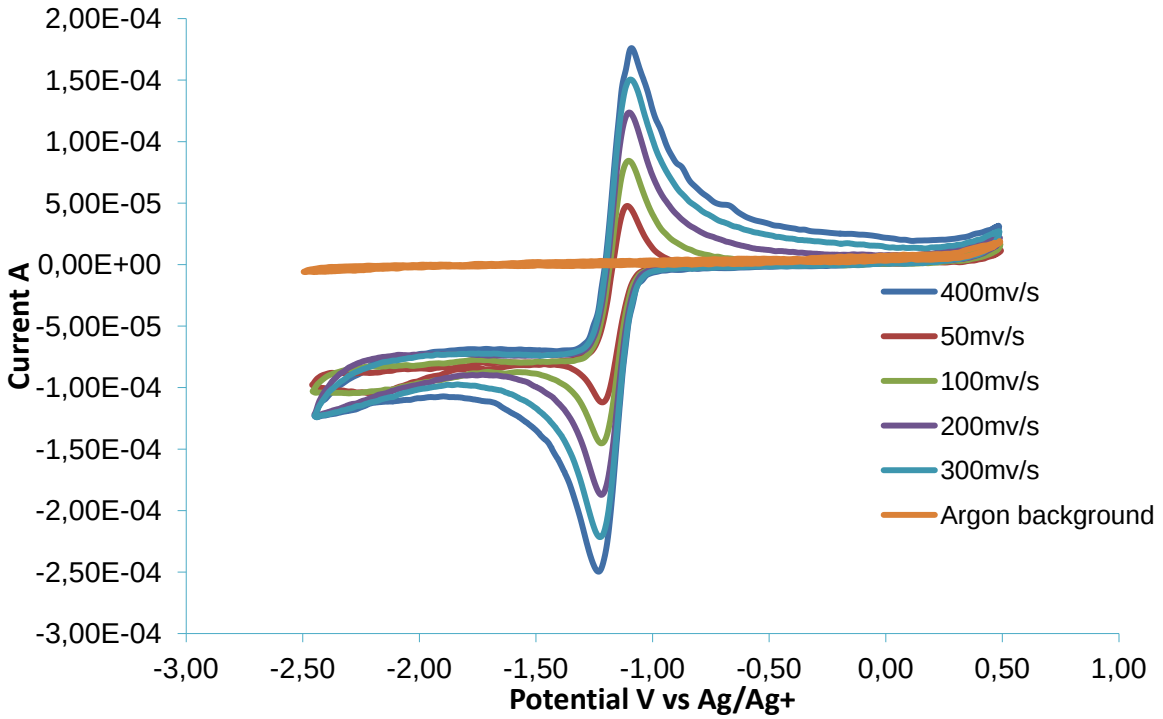

Figure 10: Cyclic voltammograms for the reduction of oxygen saturated 0.1 M $TBAPF_6$/DMSO on GC electrode at various scan rates.

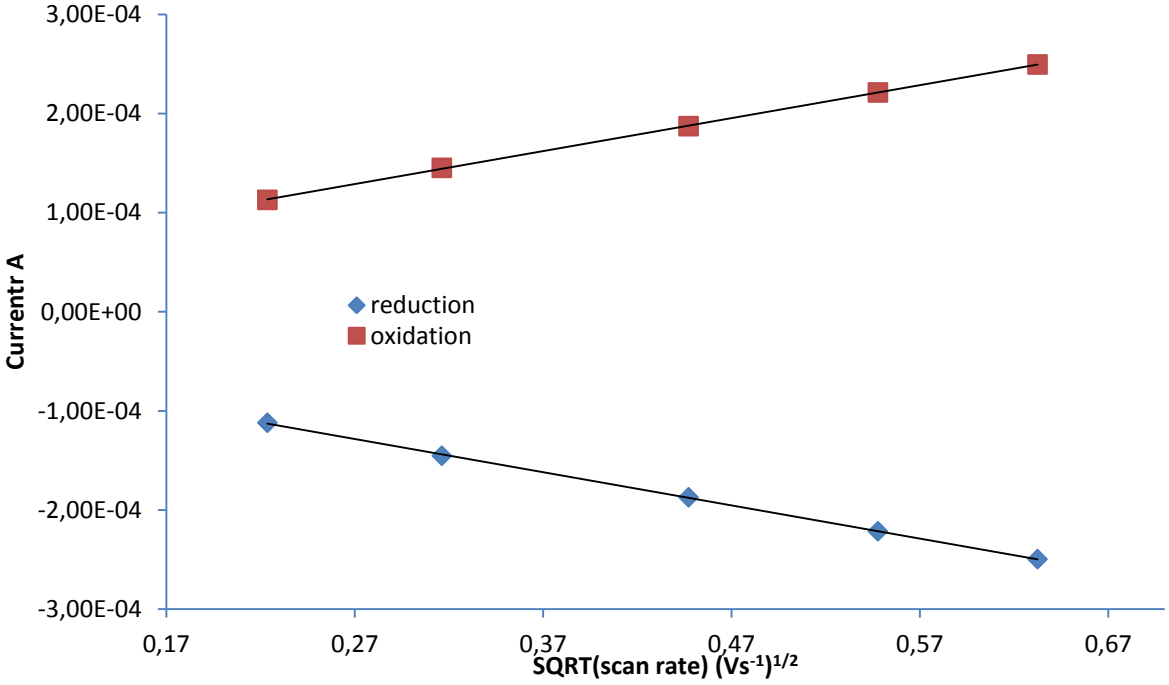

Figure 11: Randles-Sevcik plot of peak current vs square root of the scan rate in 0.1 M $TBAPF_6$/DMSO.

Diffusion coefficient for oxidation and reduction was 9.1×10^{-6} cm^2s^{-1} and 9.1×10^{-6} cm^2s^{-1} respectively. These values were calculated from Randles-Sevcik slope by using equation 2. These experimental values are very close to the values reported in literature 9.7×10^{-06} cm^2s^{-1} for oxygen reduction in DMSO (29). Kinetics of the reaction was analyzed by using eq 2 and are shown in figure 12, where Ψ is wave shape factor calculated from this equation $\Psi=24/(E-E_0)$. Figure 12 shows the variation of shape factor as function of $((D_0/D_R)^{1/4}/(\prod D_0 vF/RT)^{1/2})$. Rate constant ($k_0$) was calculated by rearranging the equation 7 where k_0 is considered as the slope of the figure 12. Rate constant for oxygen reduction in presence of 0.1M $TBAPF_6$/DMSO is $0.012 cms^{-1}$.

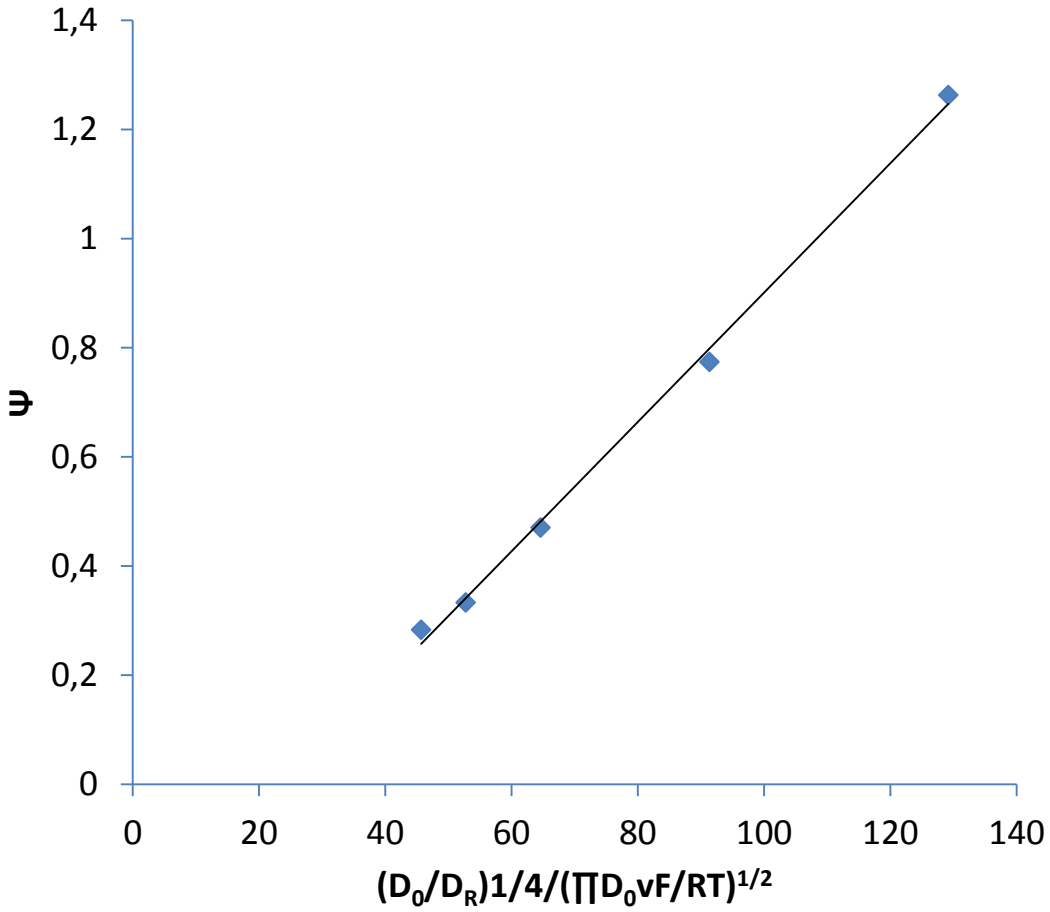

Figure 12: Variation of Ψ with scan rate, in this plot k_0 is the slope of the curve.

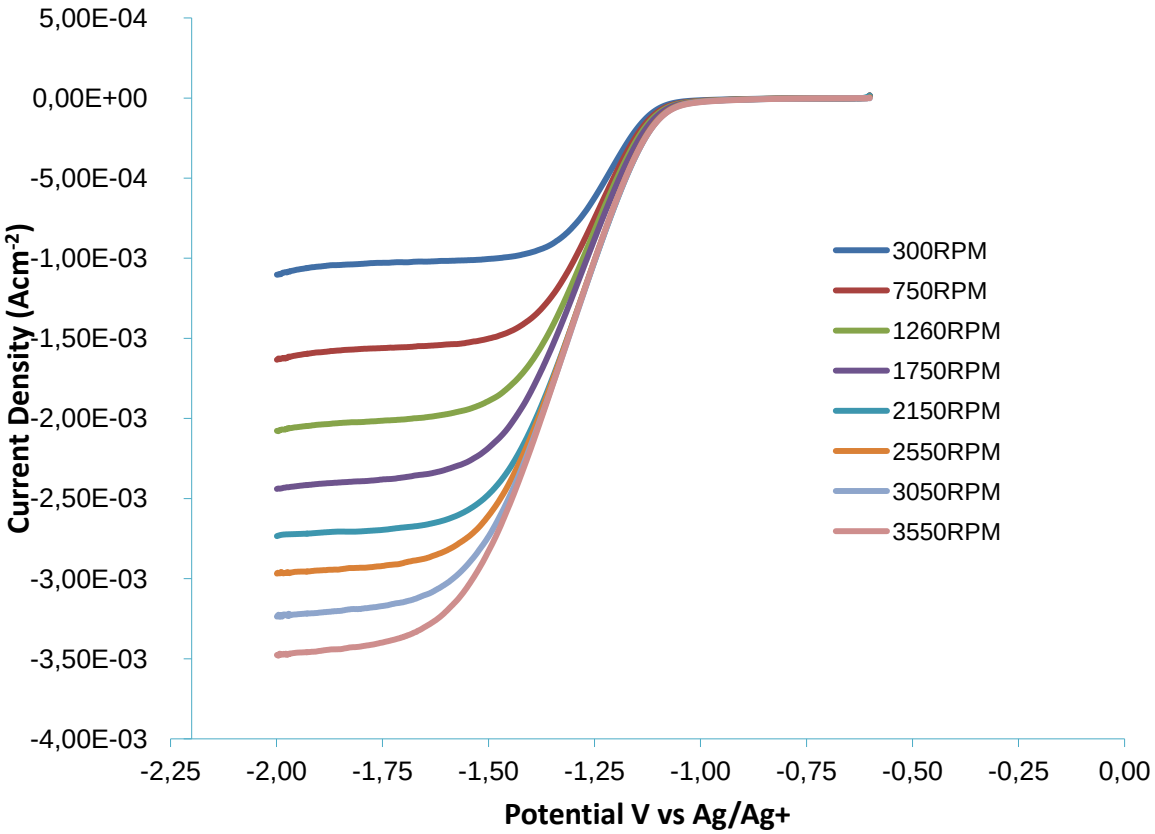

Figure 13: Rotating Disk Electrode voltammograms collected at 5mV s^{-1} in oxygenated 0.1 $MTBAPF_6$ /DMSO electrolyte at various rotation rates.

Figure 13 displays RDE voltammograms collected at 5 mV s^{-1} in oxygen saturated 0.1 $MTBAPF_6$ /DMSO electrolyte at various rotation rates. Rotating disk electrode is hydrodynamic technique which uses convection as mode of mass transport. RDE data was analyzed by using the Levich equation, which establishes a relation between current at the rotating disk and angular frequency. In the eq 5 limiting current density (I_{lim}) and n the number of electron transferred, F is the Faraday constant (96500 $Cmol^{-1}$), v is the kinematic viscosity of the solution ($1.9\times10^{-3} cm^2s^{-1}$) (29), c is concentration of oxygen (2.1×10^{-6} $molcm^{-3}$) (29) and ($\frac{2\Pi f}{60}$) is the angular frequency, Diffusion co-efficient can be calculated from the Levich equation. Levich plot given in Figure 14 indicates a mass transfer controlled electrode process. Diffusion coefficient of 9.8×10^{-6} cm^2s^{-1} calculated from Levich equation is very close to value given in literature 9.7×10^{-6} (29).

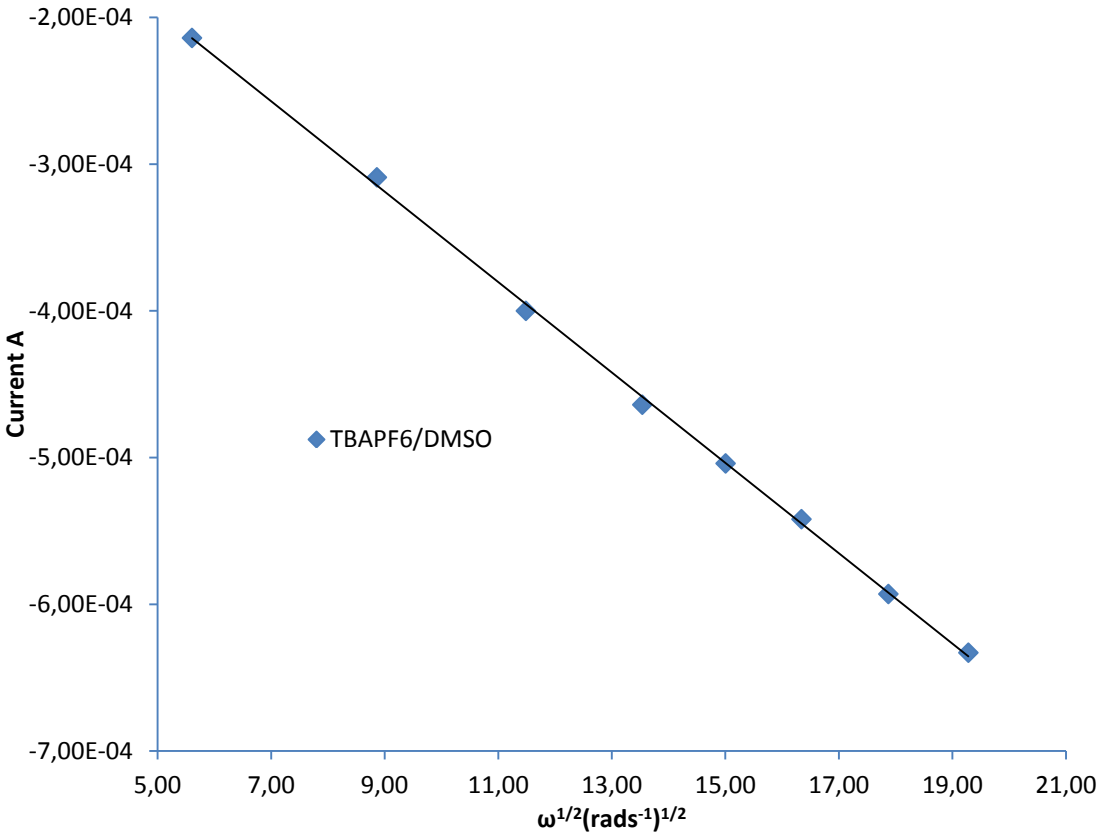

Figure 14: Levich plot of limiting current vs square root of rotation in 0.1M $TBAPF_6$/DMSO. Scan rate 5mV/s.

Reaction kinetics can be further investigated using the eq 10 & 11.

A plot of kinetic current (I_k) vs over-potential should be linear and exchange current density and over-potential can be determined from this plot. Kinetic current (I_k) can be calculated from equation 12 as given below.

$$i_k = \frac{i_{lim} i}{i_{lim} - i} \qquad \text{eq12}$$

Where i is the measured current during oxygen reduction and I_{lim} diffusion limited current from levich plot. The slope is very close to 120mVdec^{-1}.

Diffusion coefficient calculated from both experimental cyclic voltammogram (9.1×10^{-6} cm^{2}s^{-1}) and rotating disk voltammogram (9.8×10^{-6} cm^{2}s^{-1}) was very close to literature value (9.7×10^{-6} cm^{2}s^{-1}) (29). Cyclic voltammograms seem to be scan rate dependent, which is characteristic of quasi-reversible reaction. From the heterogeneous rate constant and

voltammograms peak separation it can be deduced that oxygen reduction is quasi-reversible process with high reaction rate.

4.2 Oxygen Reduction in 0.1M $TBAPF_6$/MeCN

Influence of $TBAPF_6$ on the reduction of Oxygen in MeCN was studied using CV and RDE methods**.** Ag/Ag+ reference electrode was used in these CV and RDE experiments. Cyclic voltammogram CV scanned from -2 to 0.5 V for the reduction of oxygen in 0.1M $TBAPF_6$/MeCN are presented in figure 15. Figure 15 shows the reduction of oxygen in a 0.1M $TBAPF_6$/MeCN electrolyte at 100mVs^{-1} scan rate. No appreciable current was observed under argon saturated system. The peak currents ratio for oxygen saturated voltammogram is close to unity. Oxidation peak and reduction peaks are separated by 85mV. Theoretical peak separation for one electron reversible system is 59 mV.

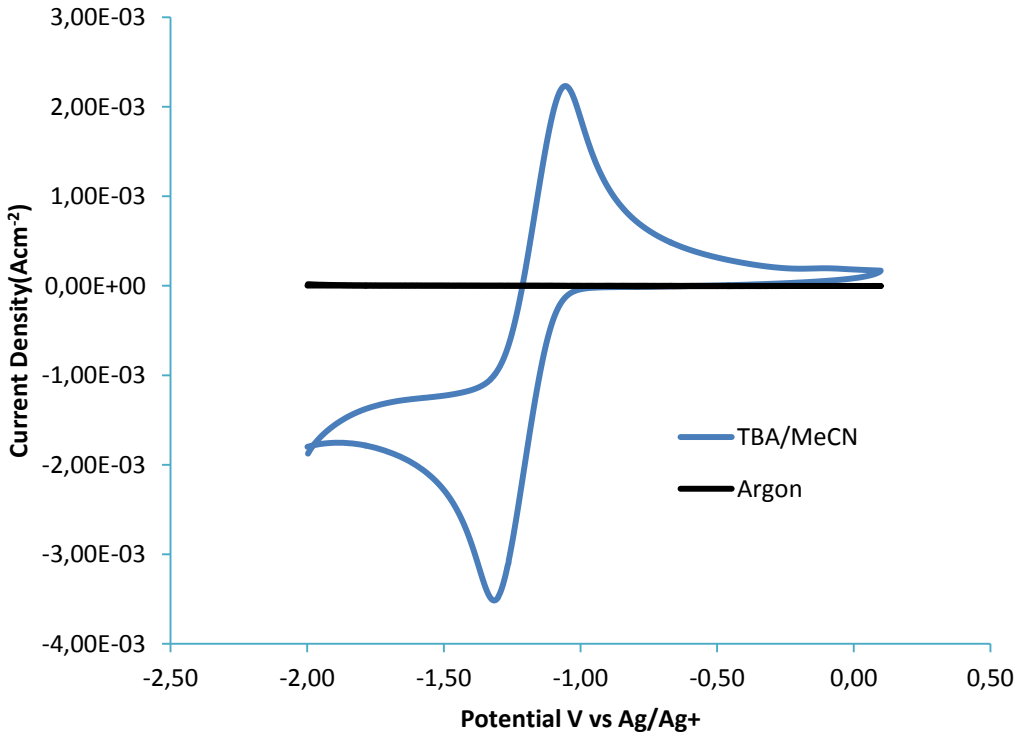

Figure 15: Cyclic voltammograms for the reduction of oxygen in 0.1M $TBAPF_6$/MeCN on a glassy carbon working electrode at a scan rate of 100mVs^{-1}.The values are IR corrected. The black curve is argon background.

In Figure 16 the cyclic voltammograms for the reduction of oxygen-saturated $TBAPF_6$/MeCN at different sweep rates are shown. The peak position is shifted with the scan rates, which is one of the characteristics of quasi reversible reaction. CV data was further analyzed by

Randles-Sevcik equation. Randles-Sevcik plot is linear which indicates the diffusion controlled electrochemical process (figure1, appendix).

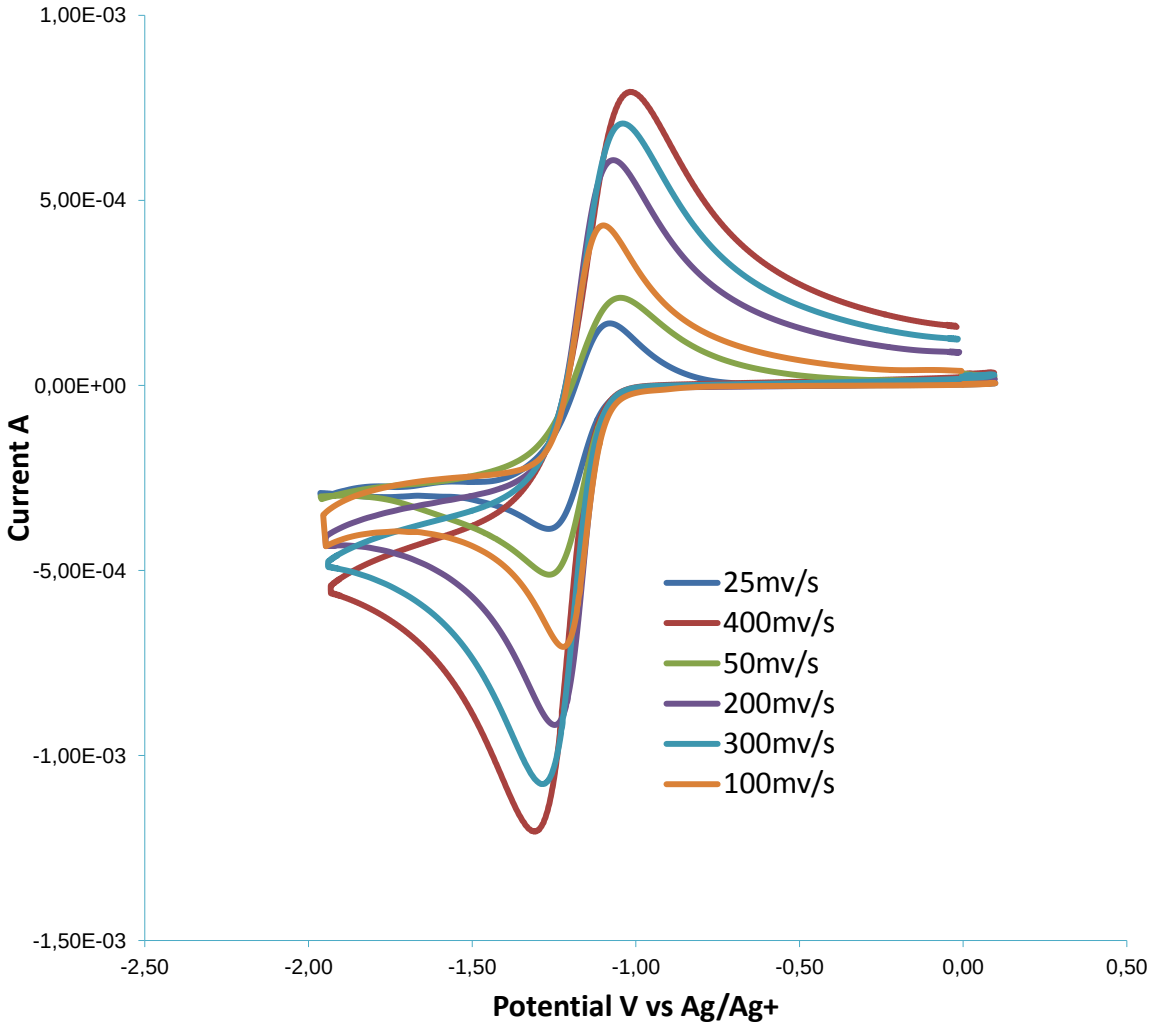

Figure 16: Cyclic voltammograms for the reduction of oxygen saturated 0.1 M $TBAPF_6$/MeCN on GC electrode at various scan rates (IR corrected).

Diffusion coefficient for oxygen reduction was 1.6×10^{-5} cm^2s^{-1} and for oxidation was 1.6×10^{-5} cm^2s^{-1}. These values were calculated from Randles-Sevcik slope using equation 2.These experimental values are very close to the literature value 2.1×10^{-5} cm^2s^{-1} (30). Kinetics of the reaction was analyzed by eq 2 and is shown in appendix figure 2. Rate constant for oxygen reduction in presence of 0.1M $TBAPF_6$/MeCN is $0.0066cms^{-1}$.

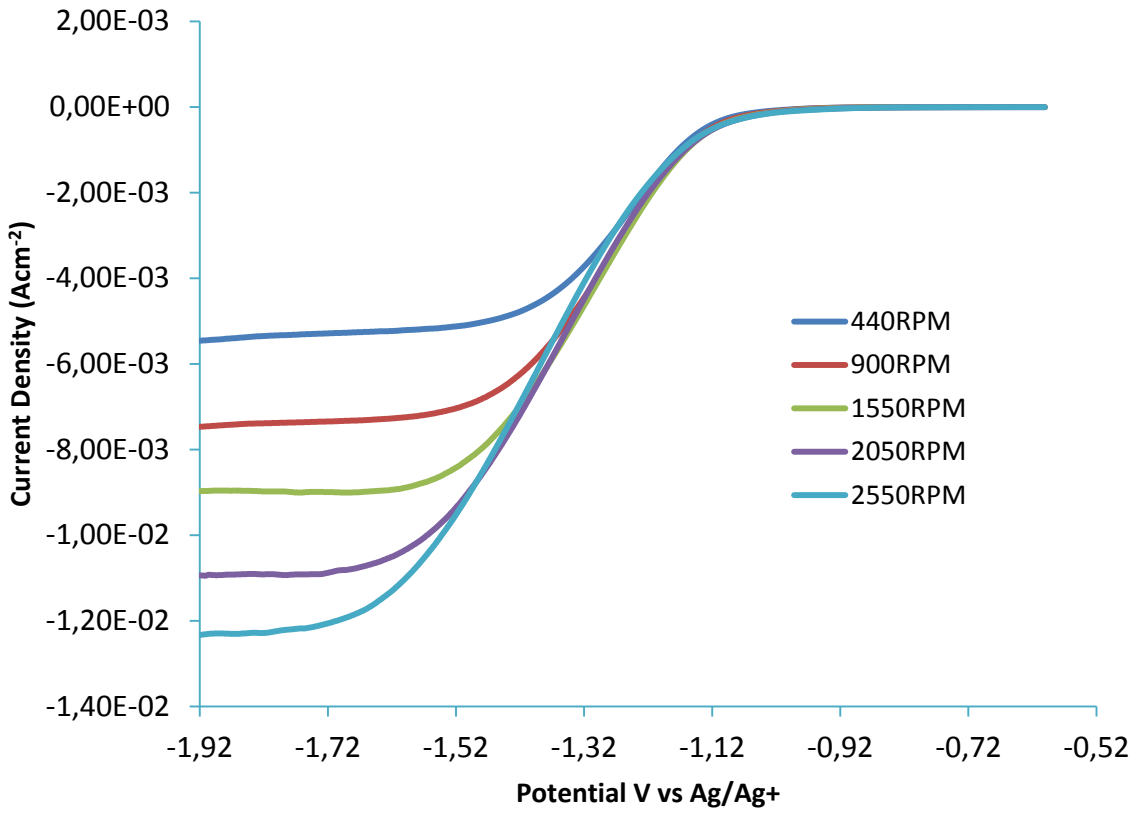

Figure 17: RDE voltammograms collected at $5mVs^{-1}$ in oxygenated 0.1 M $TBAPF_6$ /MeCN electrolyte at various rotation rates.

In Figure 17 the typical steady-state voltammograms for O_2 reduction on a RDE in oxygen-saturated 0.1 M $TBAPF_6$ solution at various rotation rates are shown. Figure 17 shows that current generation by this hydrodynamics method is higher compared to CV under diffusion control. Limiting current for the system increased with the rotation rates. From these voltammograms, it appears that there is a significant increase in the cathodic current whereas anodic current is negligible. These RDE voltammograms were further analyzed by Levich equation (eq8), where ϑ is the kinematic viscosity of the solution (4.4×10^{-3} cm^2 s^{-1}) (30) and C is the concentration of oxygen in solution (8.1 mM) (30). In Figure 18 Levich plot for the reduction of oxygen from the RDE data of limiting current density at various rotation rates is shown. Diffusion coefficient of 1.6×10^{-5} cm^2s^{-1} was calculated from eq 8 and which is very close to the value given in literature 2.4×10^{-5} cm^2s^{-1} (30). Reaction rate can be further investigated by Tafel plot. A Tafel slope for this system is very close to $120Dec^{-1}$.

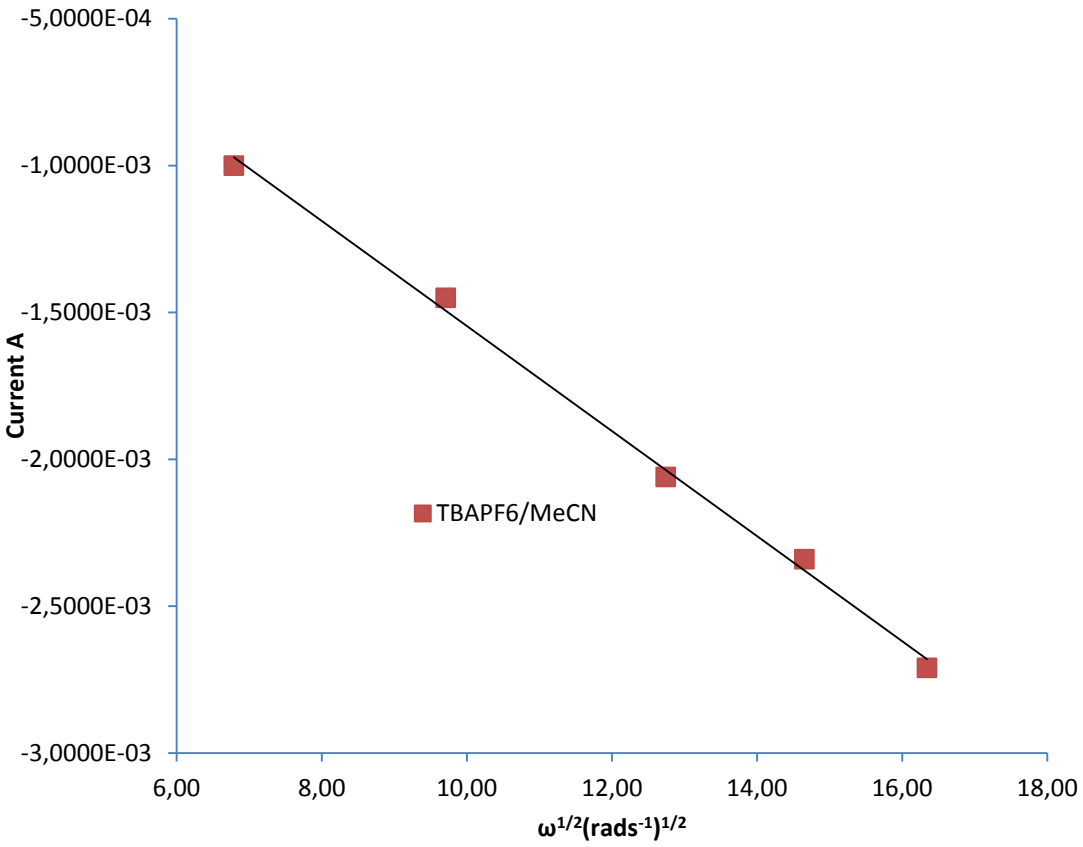

Figure 18: Levich plot of limiting current vs square root of rotation in 0.1M $TBAPF_6$/MeCN. Scan rate $5mVs^{-1}$.

The oxygen reduction reaction was analyzed for 0.1M $TBAPF_6$/MeCN system. Experimental value of diffusion coefficients of both CV and RDE method is very close to literature value (2.4×10^{-5} cm^2s^{-1}) (29). Cyclic voltammograms seem to be scan rate dependent and which is a characteristic of a typical quasi-reversible reaction. Therefore, oxygen reduction to form superoxide is one electron quasi-reversible process. Heterogeneous rate constant value is close to the value found for 0.1M $TBAPF_6$/DMSO system.

4.3 Oxygen Reduction in 0.1M $LiPF_6$/DMSO

Influences of $LiPF_6$ on the reduction of Oxygen in DMSO were studied using CV and RDE methods using glassy carbon as working and Ag/Ag+ as reference electrodes. Oxygen reduction mechanism in $LiPF_6$ containing electrolytes was different from $TBAPF_6$ containing electrolytes. Figure 19 illustrates O_2 reduction in 0.1M $LiPF_6$/DMSO at 100mVs^{-1} scan rate. No appreciable current was observed under argon saturated system. However, in O_2 saturated system very large reduction peak current is seen compared to the oxidation peak current. The reduction peak potential is -1.27V and the oxidation peak potential is -0.316V. Peak separation is very large compared to the $TBAPF_6$/DMSO, despite the fact that both systems contain same solvent. The calculated half peak potential is -1.18V. For one electron reversible process, potential difference between cathodic peak and half-peak potential (potential at the half-value of the peak current) is 56.5 mV (25). For the investigated $LiPF_6$/DMSO system the potential difference is about 90mV at 100mVs^{-1} scan rate, which indicates more complex processes occurring than just reversible processes.

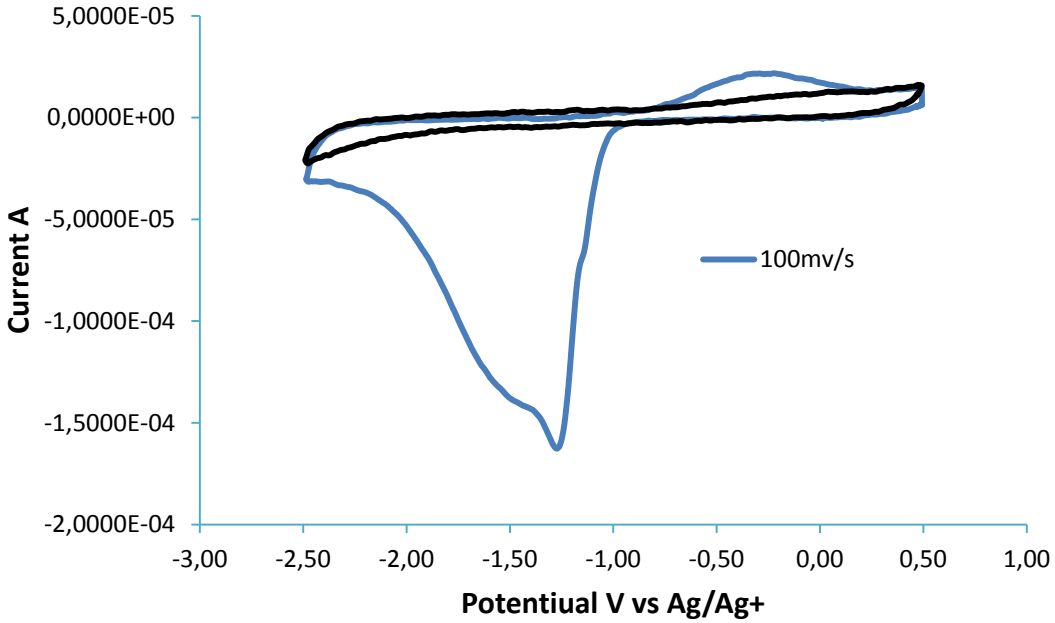

Figure 19: Cyclic voltammograms for the reduction of oxygen in 0.1M $LiPF_6$/DMSO on a glassy carbon working electrode at a scan rate of 100mVs^{-1}.The values are IR corrected. The black curve is argon background.

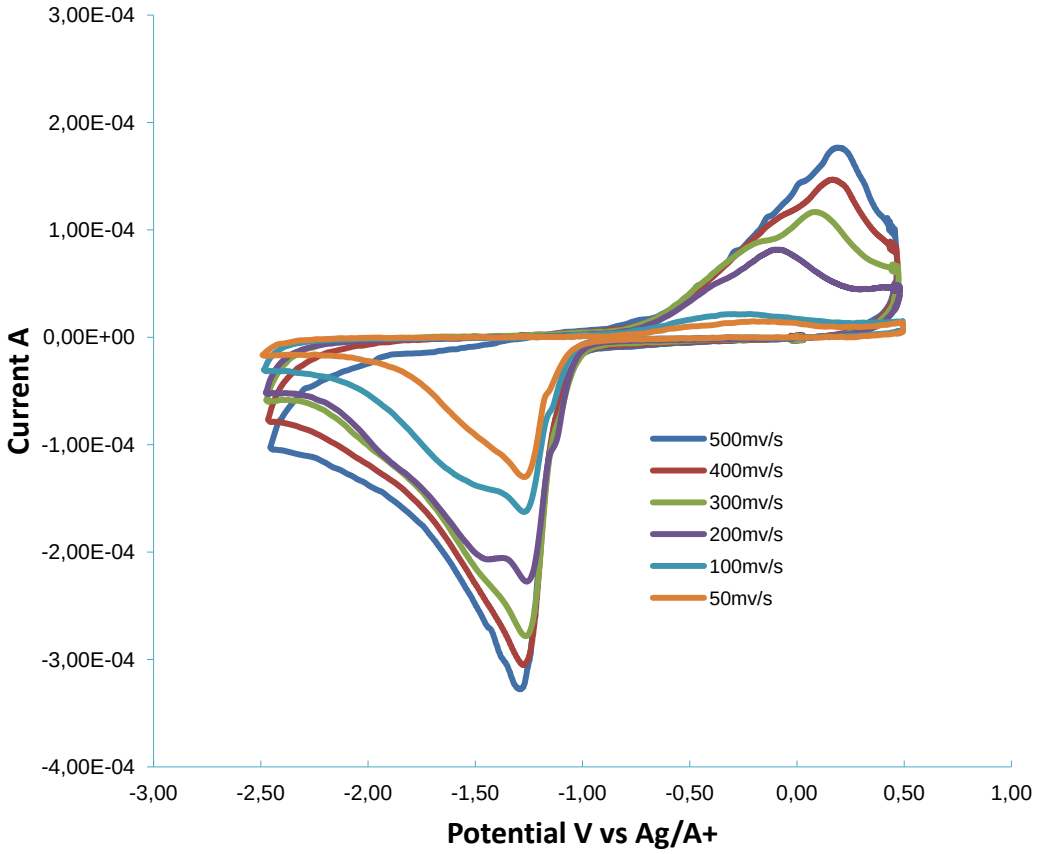

Figure 20: Cyclic voltammograms for the reduction of oxygen saturated 0.1 M $LiPF_6$/DMSO on GC electrode at various scan rates.(IR corrected).

Figure 20 shows, the cyclic voltammograms for the reduction of oxygen-saturated 0.1M $LiPF_6$/DMSO at different sweep rates. The peak position is shifted with the scan rates. Scan rate dependency which is observed in this system is one of the characteristics of quasi reversible system or irreversible system. CV data was further analyzed by the Nicholson & Shain relationship (eq 6), where, transfer coefficients α (0, 5), diffusion coefficient of the oxygen D ($1.6\times10^{-5}cm^2s^{-1}$) were used (29). Nicholson & Shain plot is linear and number of electron involved in this reduction process is one which is determined from eq 6 (figure 21). However, in these voltammograms more than one reduction and oxidation peaks are apparent which are more obvious at lower scan rate than higher scan rates. The first reduction process could be the formation of superoxide, which further reduced to another reduced form of oxygen.

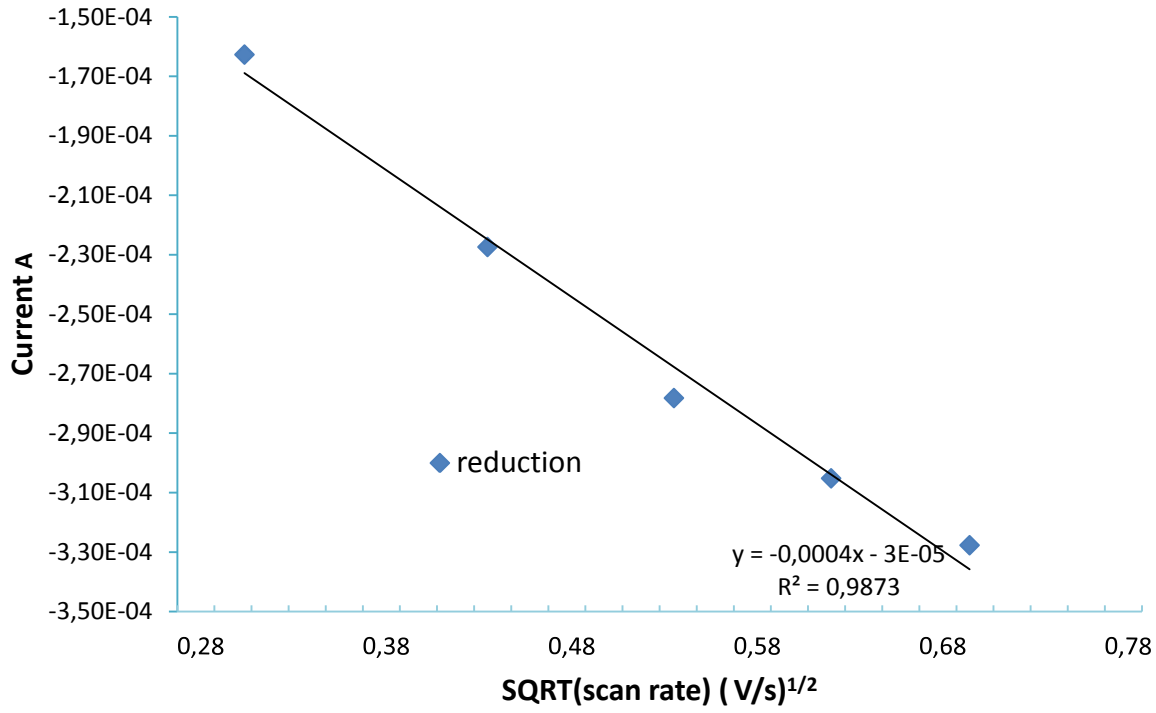

Figure 21: Peak current vs. square root of the scan rate in 0.1 M $LiPF_6$/DMSO.

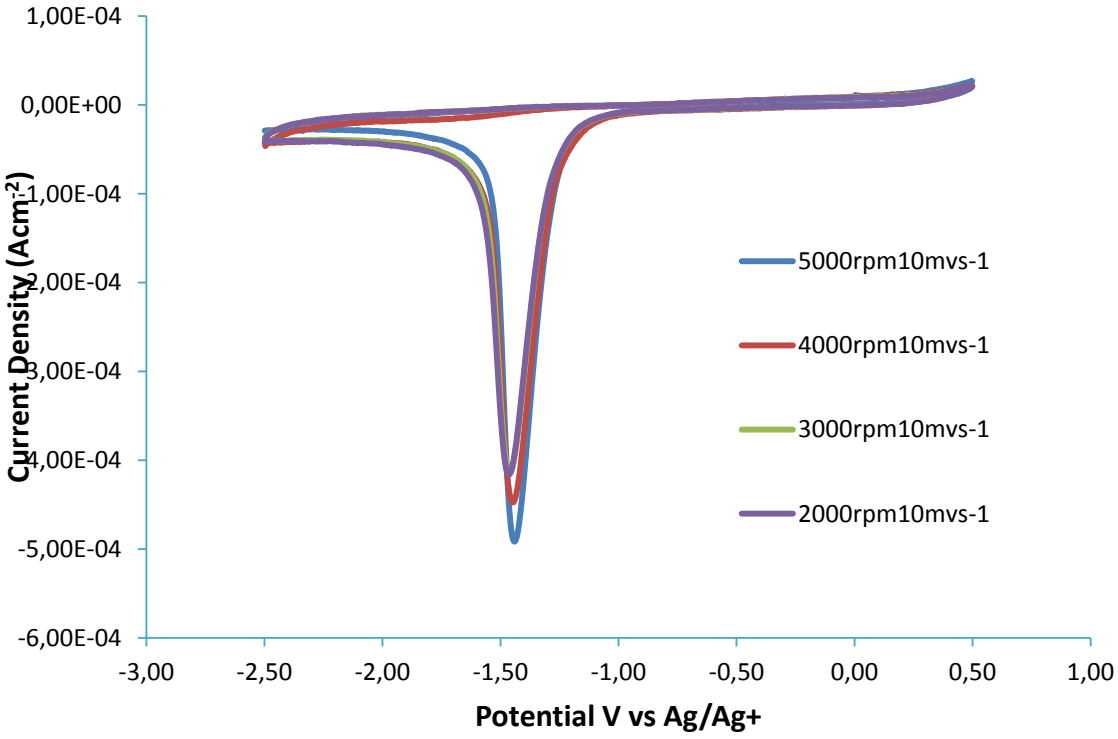

Figure 22: Rotating Disk Electrode voltammograms collected in oxygenated 0.1 M $LiPF_6$ /DMSO at various rotation rates.

Further investigation of the reduction process was conducted via rotating disk electrode (RDE) voltammetry and results are shown in Figure 22. These RDE experiments were conducted at $10mVs^{-1}$ scan rate. Excessive amount of insulating product deposited after every run on the working electrode and that deposit had to be removed before further use.

Moreover, cyclic voltammograms show scan rate dependency. Because several peaks appeared in the cyclic voltammograms. Here, oxygen reduction is one electron reduction accompanied with chemical follow-up reactions. In presence of Li^+ ion L_2O_2, Li_2O could form during discharge process. These insulating products deposit on electrode surface and block the reaction sites of electrode surface. These discharge products cannot be removed from the electrode surface by electrochemical cycling. Therefore, the oxidation process is even more complex and difficult to analyze.

4.4 Oxygen Reduction in 0.1M $LiPF_6$/MeCN.

In Figure 23 the cyclic voltammograms for the reduction of oxygen-saturated 0.1M $LiPF_6$/MeCN at different sweep rates are shown. The peak position is shifted with the scan rates and no significant oxidation peak is observed. Oxygen reduction in presence of $LiPF_6$/MeCN is very slow and the process seems to be irreversible.

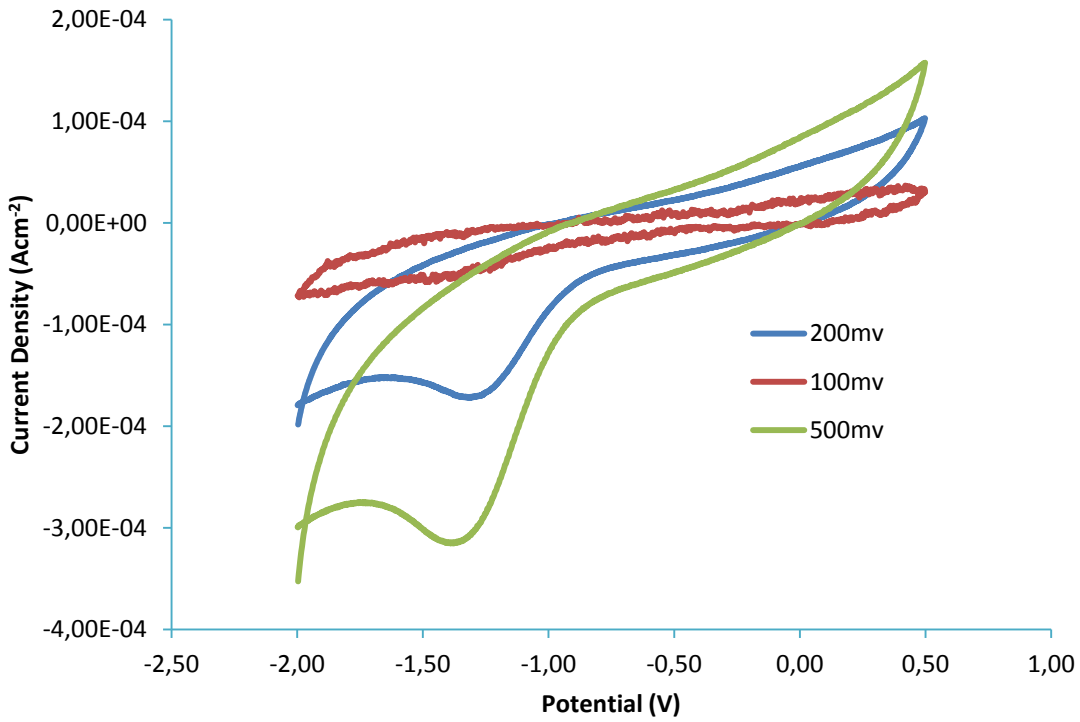

Figure 23: Cyclic voltammograms for the reduction of oxygen saturated 0.1 M $LiPF_6$/MeCN on GC electrode at various scan rates.

4.5 Oxygen Reduction in 0.1M $LiClO_4$/DMSO

Results of the ORR in 0.1M $LiClO_4$/DMSO solution are shown in Figure 24. The oxidation peak current is very low compared to the reduction peak current. The reduction peak potential is -1.2 V and oxidation peak potential is 0.2V . Peak separation is very large compared to TBA system and even larger than $LiPF_6$ in DMSO which leads to irreversible oxygen transfer reaction. Half peak potential of the system is -1.12V . The potential difference between cathodic peak and half peak potential is 80mV. For one electron reversible reaction the potential difference between cathodic peak and half-peak potential (potential at the half-value of the peak current) is 56.5mV (25). This 80mV of potential difference demonstrates complex process than a reversible process.

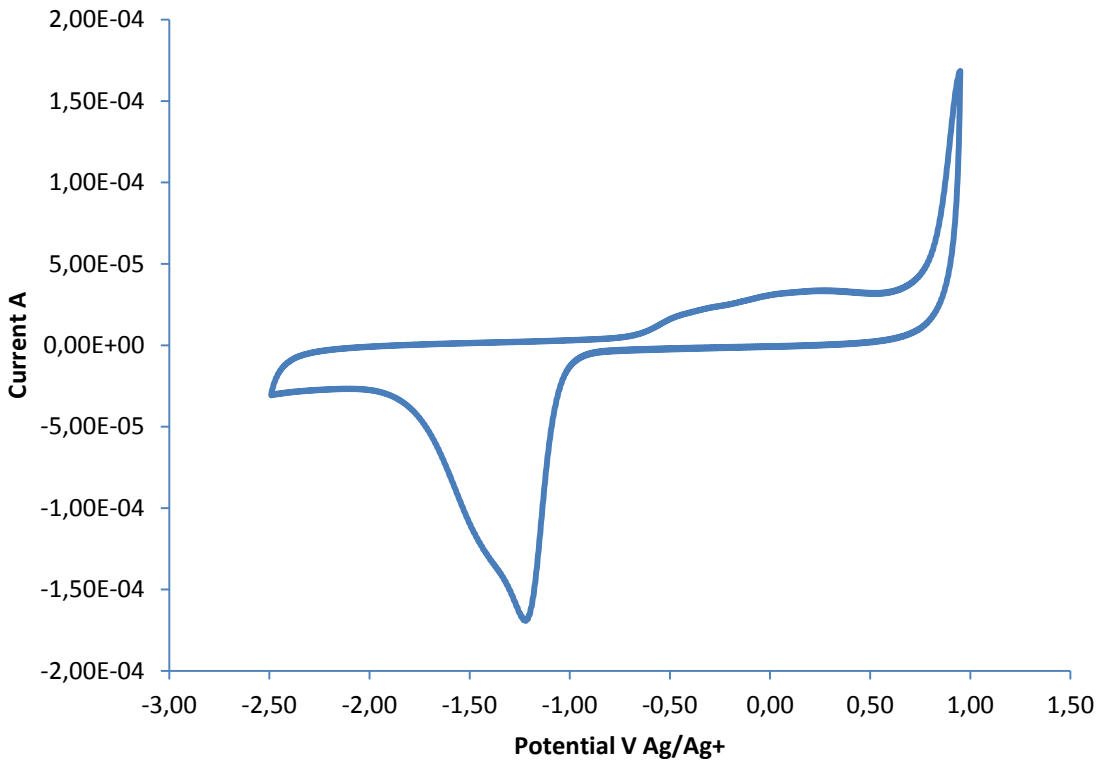

Figure 24: Cyclic voltammograms for the reduction of oxygen in 0.1M $LiClO_4$/DMSO on a glassy carbon working electrode at a scan rate of 100mVs^{-1}.The values are IR corrected.

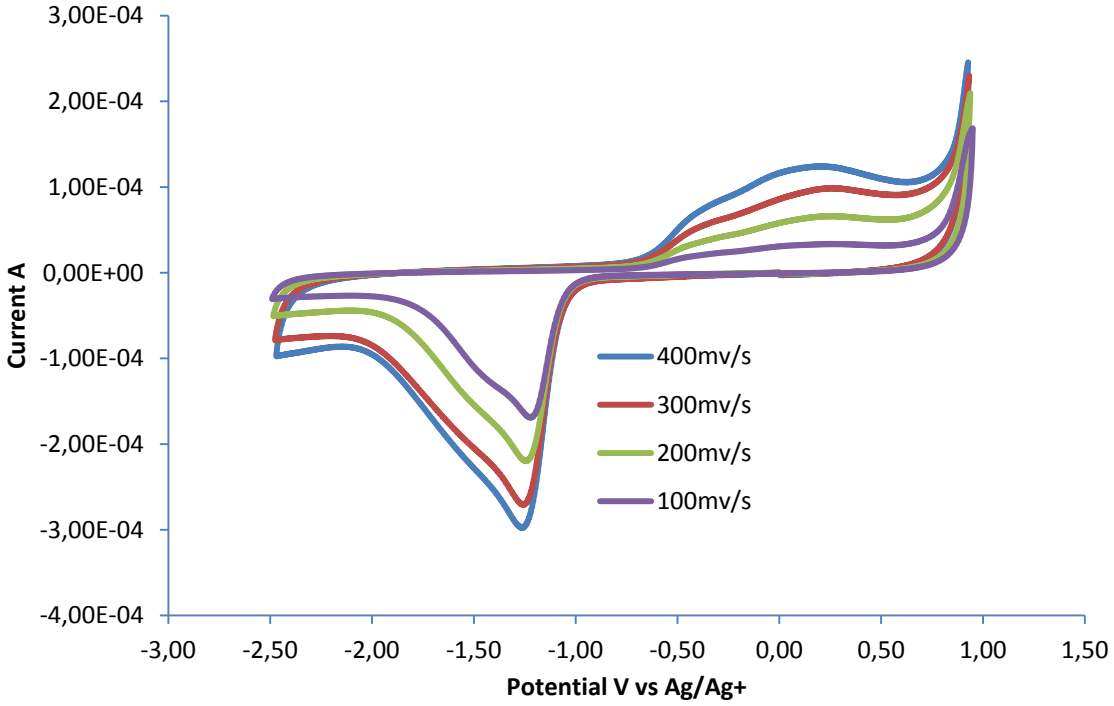

Figure 25: Cyclic voltammograms for the reduction of oxygen saturated 0.1 M $LiClO_4$/DMSO on GC electrode at various scan rates.

Figure 25 shows, the cyclic voltammograms for the reduction of oxygen-saturated 0.1M $LiClO_4$/DMSO at different sweep rates. As seen in the case of $LiPF_6$/DMSO the peak position is shifted with the scan rates which is one of the characteristics of quasi-reversible or irreversible system. CV data was further analyzed by the Nicholson & Shain relationship (eq 6), Experimental plot is linear and number of electron involved in this reduction process is one (figure 3, appendix).

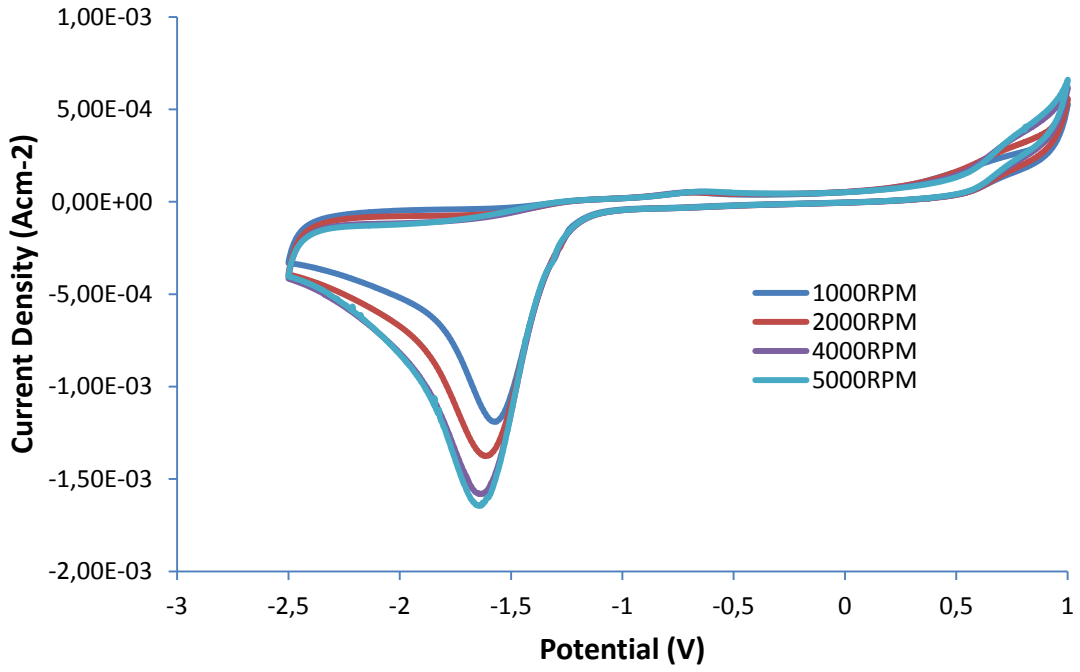

Figure 26: Rotating Disk Electrode voltammograms collected at $10mVs^{-1}$ in oxygenated 0.1 M $LiClO_4$ /DMSO electrolyte at various rotation rates.

In Figure 26 the reduction process analyzed via rotating disk electrode (RDE) voltammetry is shown. These RDE experiment were conducted at $10mVs^{-1}$ scan rate and various rotation rates. Cyclic voltammograms seem to be scan rate dependent. The oxygen reduction process seems to be one electron reduction with follow-up chemical reactions. The oxidation process is complex and difficult to analyze. Passivation is associated with the ORR in the presence of Li^+ ion in DMSO solvent. Due to the deposition of insoluble reduction products on to the surface of the working electrode blocks reaction sites and these products cannot be removed by electrochemical cycling. A continuous decrease of the reduction peak current was obtained over multiple cycles.

4.6 Oxygen Reduction in 0.1M $LiClO_4$/MeCN

Figure 27 shows, the cyclic voltammograms for the reduction of oxygen-saturated 0.1M $LiClO_4$/MeCN at different sweep rates. The peak position is shifted with the scan rates. No significance oxidation peak is observed. Reduction of oxygen in presence $LiPF_6$/MECN is very slow. No oxidation peak was observed and the process seems to be irreversible.

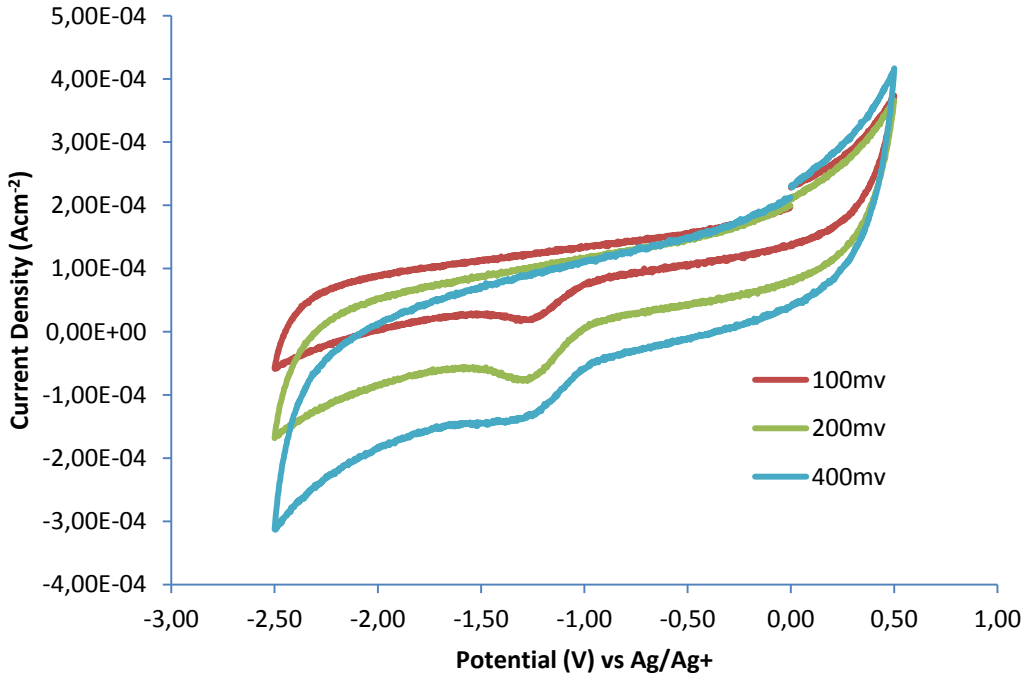

Figure 27: Cyclic voltammograms for the reduction of oxygen saturated 0.1 M $LiClO_4$/MeCN on GC electrode at various scan rates.

4.7 Oxygen Reduction in mixed $LiPF_6$ and $LiClO_4$ system in DMSO

Mechanism of oxygen reduction for mixed Lithium salts 0.1M (70%$LiClO_4$+30% $LiPF_6$, 80% $LiClO_4$+20% $LiPF_6$, 90% $LiClO_4$+10% $LiPF_6$) in DMSO was investigated. In Figure 28 CV curves of pure and mixed systems are compared. The value of the reduction peak current for mixed system is lower compared to 0.1M $LiPF_6$/DMSO and 0.1M$LiClO_4$/DMSO but secondary reduction peaks disappeared. Oxidation process seems to be more complex according to CV curves. Moreover, the reduction peak currents were gradually increased with the increase of $LiClO_4$ concentration.

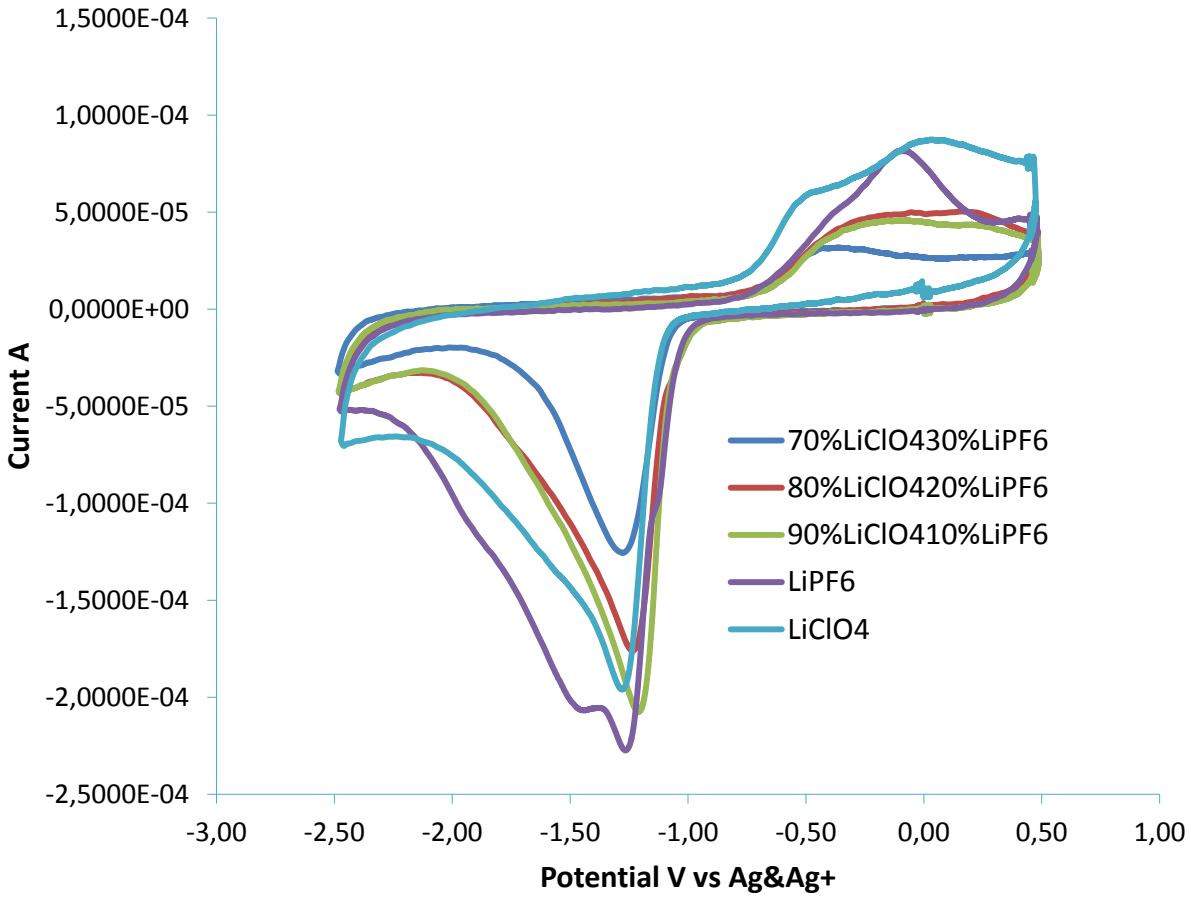

Figure 28: Cyclic voltammograms for the reduction of oxygen saturated 0.1 M Li based mixed salt/DMSO on GC electrode at 200mVs^{-1} scan rate.

4.8 Oxygen Reduction in mixed $LiPF_6$ and $TBAPF_6$ system in DMSO

Oxygen reduction in DMSO was also investigated for mixtures of $TBAPF_6$ and $LiPF_6$ salts. Mixed systems are 0.1M (80%TBA+20%20$LiPF_6$), 0.1M (70%TBA+30%20$LiPF_6$) and 0.1M (50%TBA+50%$LiPF_6$). Figure 29 displays, CV comparison of mixed TBA, $LiPF_6$ systems with pure $TBAPF_6$, $LiPF_6$ systems. The reduction peak current for 0.1M (50%TBA+50%$LiPF_6$) is higher compared to pure systems as well as compared to other mixed systems. On the other hand, the reduction peak currents for other mixed systems are lower compared to pure Li systems. However, secondary reduction peaks disappeared. Oxidation peaks are similar for pure Li and mixed systems.

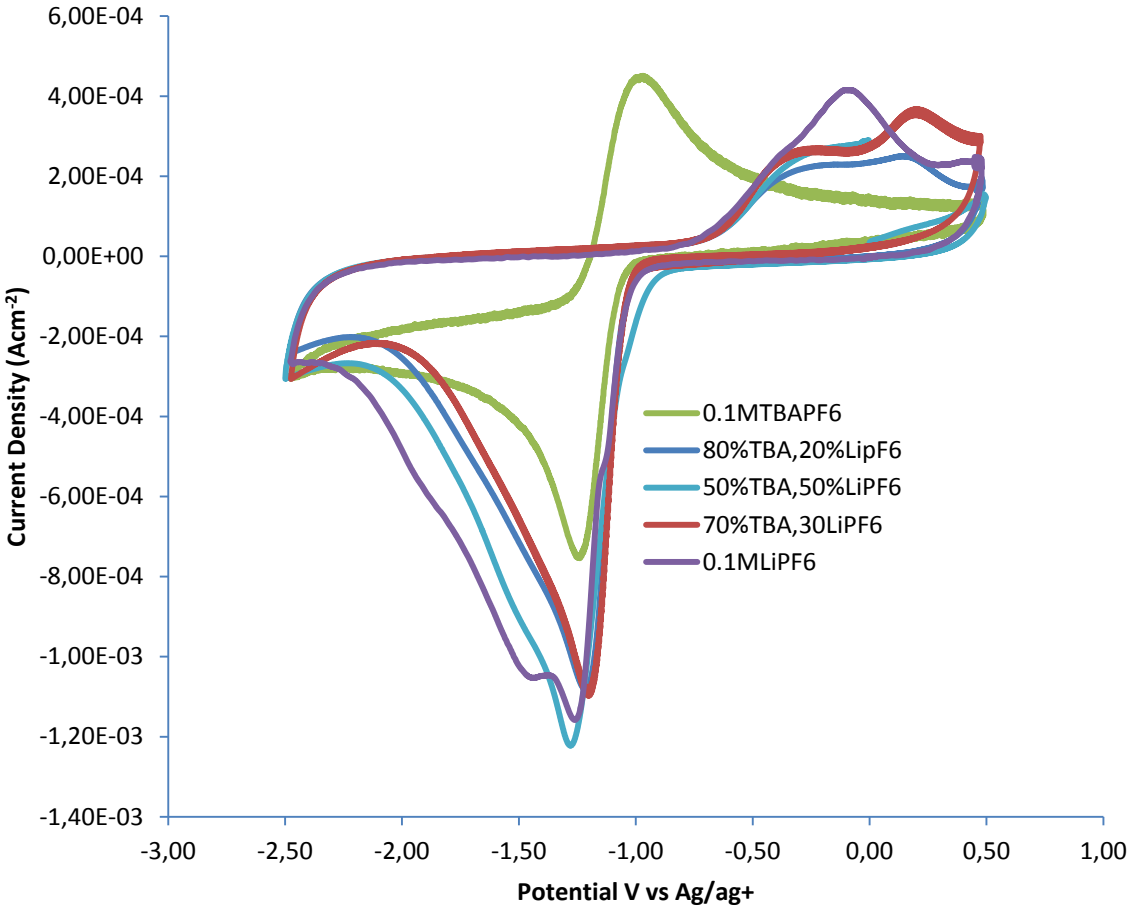

Figure 29: Cyclic voltammograms for the reduction of oxygen saturated 0.1 M mixed ($LiPF_6$+$TBAPF_6$ salt) in DMSO on GC electrode at 200mvs^{-1} scan rate.

4.8 Comparison of the oxygen reduction reaction kinetics in different electrolytes

The ORR mechanism in $TBAPF_6$/DMSO and in $TBAPF_6$/MeCN is one electron reduction of oxygen to superoxide ($O_2^{\cdot-}$) and subsequent re-oxidation of superoxide to oxygen. Reaction mechanism of oxygen reduction can be described by reaction scheme shown below;

Reduction: $O_2 + e^- \rightarrow O_2^{\cdot-}$

Oxidation: $O_2^{\cdot-} \rightarrow O_2 + e^-$

In Table 2 kinetic properties of different systems investigated in this study are compared. According to the values of heterogeneous rate constant the oxygen reduction reaction is quasi-reversible in DMSO and also in MeCN. However, in the presence of TBA^+ ion in DMSO

the value of heterogeneous rate constant of oxygen reduction is higher than that in MeCN and these calculated values are close to literature values (29). In the presence of $LiPF_6$ and $LiClO_4$ oxygen reduction seems to be slower. Tafel slopes for TBA in DMSO and MeCN were closer to $120Dec^{-1}$.

Table 4: Kinetics properties of oxygen saturated different electrolytes.

electrolyte	**Experimental diffusion coefficient (cm^2/s)**	**Heterogeneous rate constant k_o (cms^{-1})**	**Literature diffusion coefficient (cm^2/s)**	**Literature value of Heterogeneous rate constant k_o (cms^{-1})**
0,1M $TBAPF_6$ in DMSO	9.8×10^{-6}	0.012	9.7×10^{-6} (29)	($*4\times10^{-2}$ - 4×10^{-3})(29)
0,1M $TBAPF_6$ in MeCN	1.6×10^{-5}	6.6×10^{-3}	2.4×10^{-5}(29)	($*3\times10^{-3}$ - 6×10^{-4})(29)

Oxygen reduction in mixed Li electrolytes in DMSO solvent is more complex than pure Li systems. Several reduction peaks disappeared although the value of reduction current peaks decreased. Oxidation process is even more complex than the reduction process in mixed electrolyte systems.

Rate constant not only depends on diffusion coefficient but also on the peak potential separation. Comparing the CV of $TBAPF_6$/DMSO (figure 10) and $TBAPF_6$/MeCN (figure 16) with $LiPF_6$/DMSO (figure 20) and $LiPF_6$/MeCN (figure 23) it is clear that peak separation of TBA based electrolyte is quite less than Li based electrolytes. More clear information about the rate constant can be obtained according to the suggested zone boundaries for rate constants by Matsuda and Ayabe's.

Reversible $\Lambda \geq 15$; $k_0 = 0{,}3\,\vartheta^{1/2}$ cms^{-1}

Quasi-reversible $15 \geq \Lambda \geq 10^{-2(1+\alpha)}$; $0{,}3\,\vartheta^{1/2} \geq 2\times10^{-5}\vartheta^{1/2}$ cms^{-1}

Totally irreversible $\Lambda \leq 10^{-2(1+\alpha)}$; $k_0 \leq 2\times10^{-5}\vartheta^{1/2}$ cms^{-1}(26).

Oxygen reduction rate constant value of 0.1M $TBAPF_6$ in DMSO and MeCN is in the quasi-reversible range, their peak potentials are scan rate dependant. That's why, oxygen reduction in presence of TBA^+ ion is quasi-reversible. Heterogeneous rate constant for the ORR of oxygen in the presence of Li^+ ion could not be determined, because reduction process was accompanied with multiple reduction and chemical follow-up reactions. Deposition of discharge product on electrode surface blocked the reaction sites which resulted in a decrease of discharge capacity for subsequent cycles.

Chapter 5

Conclusions and Future works

Oxygen reduction mechanism was investigated in organic solvents which are relevant for the rechargeable Li-air battery. Role of different supporting electrolytes i.e., $TBAPF_6$, $LiPF_6$ and $LiClO_4$ on oxygen diffusivity and reduction mechanism in DMSO and MeCN was analyzed. Oxygen reduction and subsequent oxidation strongly influenced by the type of solvent and also by the nature of cation. Oxygen reduction in DMSO in the case of TBA^+ PF_6^- ions in DMSO as well as in MeCN was quasi-reversible with fairly high heterogeneous rate constant. This indicates a profound effect of cation interaction with the solvent on the oxygen diffusivity. $LiClO_4$ has pronounced drawback of forming passivation layer on electrode. It was not possible to analyse the oxidation process due to the occurrence of multiple processes during oxidation. Oxygen reduction in mixed supporting electrolytes ($LiClO_4$+$LiPF_6$) was quite complex. Extra reduction peaks disappeared in the cyclic voltammetry of mixed salts based electrolytes. It might be the case that mixed electrolytes may have influence in the dissolving of reduction products.

In future studies should be performed with appropriate catalyst to improve oxidation process. Catalyst can help to dissolve the reduction products and accelerate oxygen reduction process. Pd mixed with MnO_2 and CeO_2 could be used as catalysts. As we have seen in this work that nature of electrolytes have great influence on the oxygen reduction process, therefore new class of non-aqueous electrolytes need to be developed. Ionic liquid could be a good choice to improve the reversibility of the Li-air battery.

Appendix

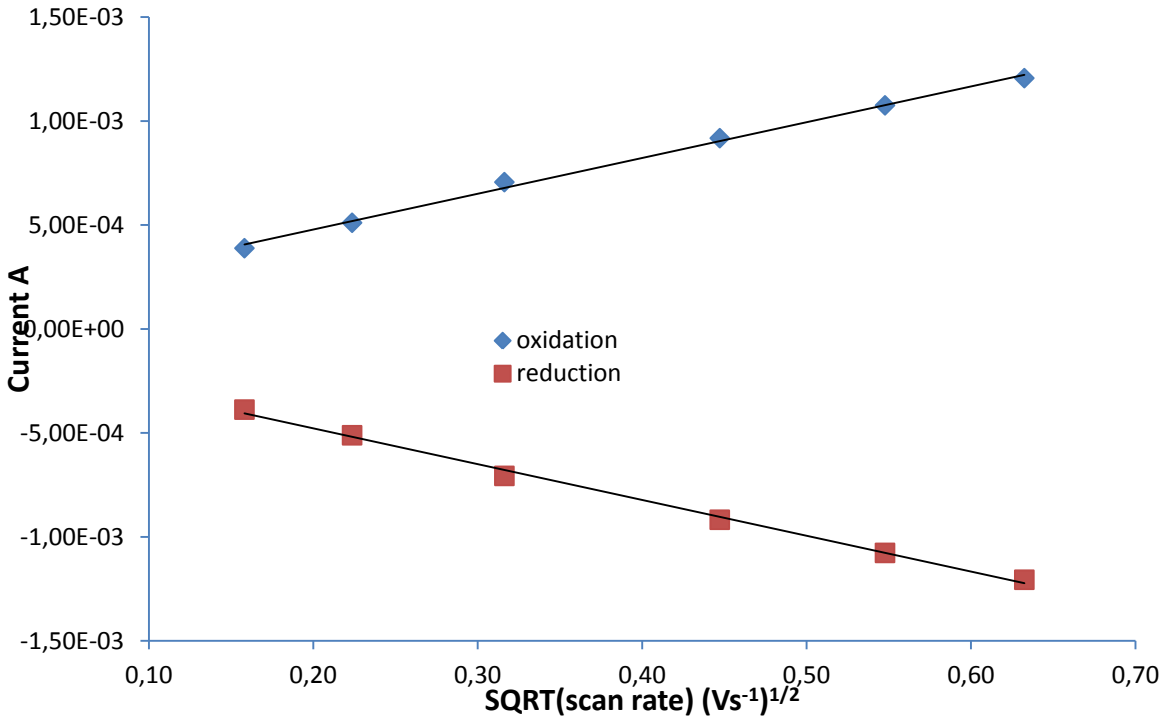

Figure 1: Randles-Sevcik plot of peak current vs square root of the scan rate in 0.1 M $TBAPF_6$/MeCN. Blue rectangle line is experimental oxidation plot and red rectangle line is experimental reduction plot.

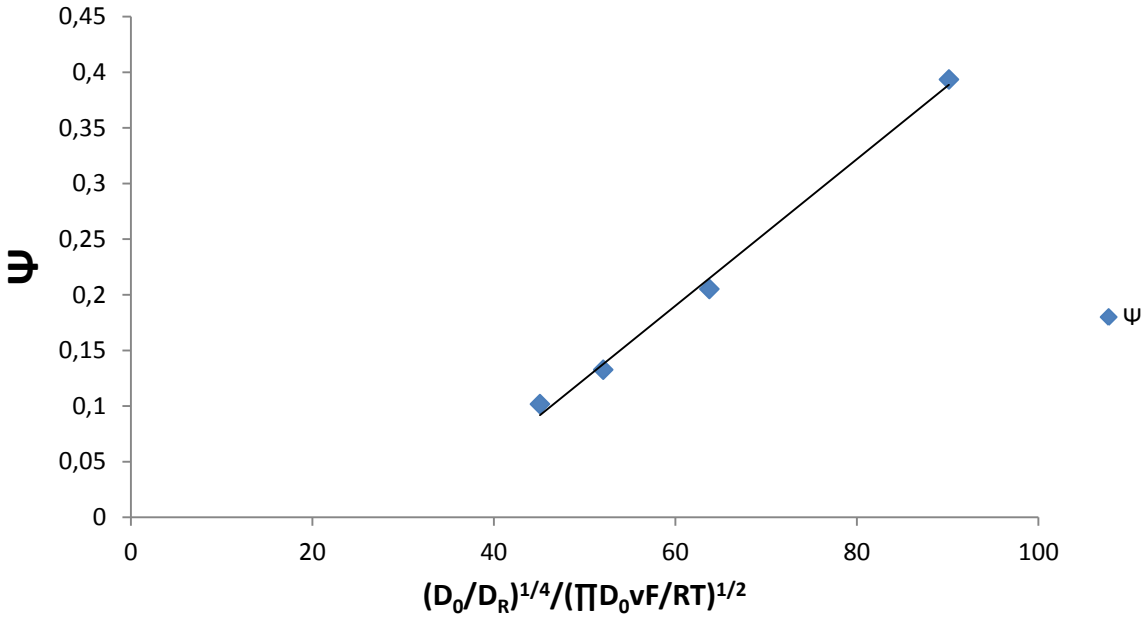

Figure 2: A plot of variation of wave shape factor Ψ with scan rate, in this plot k_0 is the slope of the curve for in 0.1 M $TBAPF_6$/MeCN.

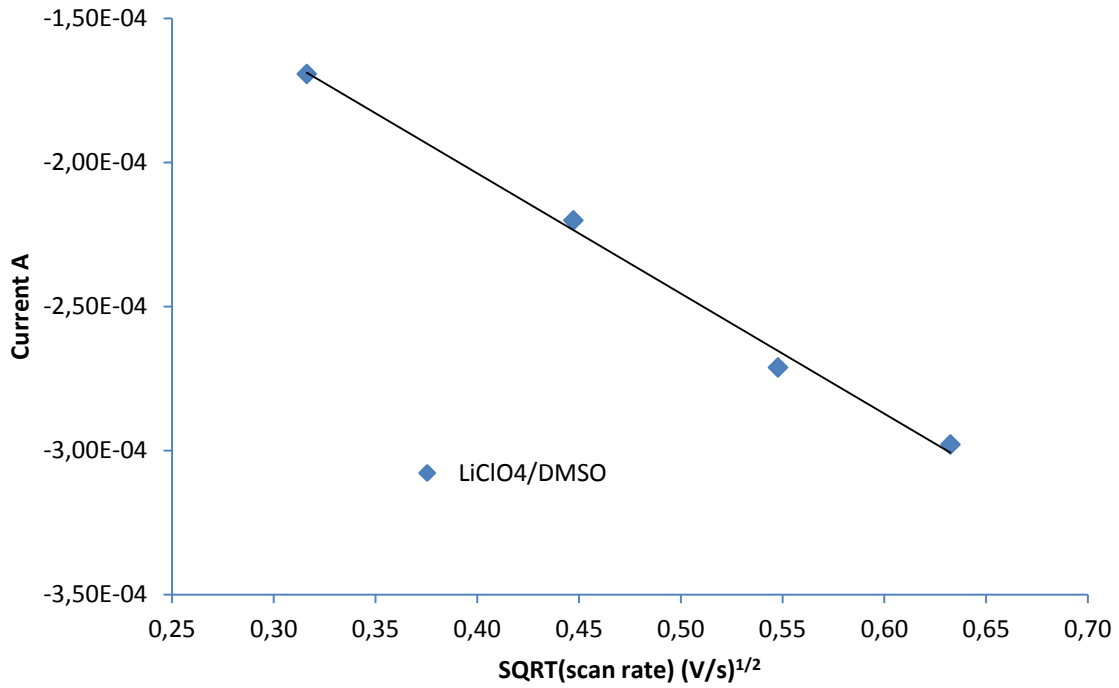

Figure 3: Peak current vs. square root of the scan rate in 0.1 M $LiClO_4$/DMSO. Red rectangle line is theoretical plot of one electron reduction.

Acknowledgements

This work has been done in the Laboratory of electrochemistry. I would like to sincerely thank my supervisor associate professor Zareen Abbas for his constructive help in theoretical and practical studies. Without his help it would not have been possible to successfully done this project. I would also like to thank my examiner Professor Elisabet Ahlberg for giving me an opportunity to work in electrochemistry group and helping me to analyze the kinetics of reactions.

I would like to thanks PHD students Gert Göransson, Adriano S. O. Gomes and Kristopher Hedenstedt for helping me with the instrumentation and software. Without their help it would be difficult for me to work in the lab.

I also would like to thanks my supervisor from Volvo Technology Senior Research Engineer Istaq Ahmed for assisting me with the requirements as well as giving me the support needed for this project. Last but not least, I would like to special thanks to Volvo for giving me fund for this project.

References

1. Fuminori Mizuno , Shinji Nakanishi, Yukinari Kotani, Shoji Yokoishi, Hideki Iba, Electrochemistry (2010) , 5, 403-405.
2. http:/large.stanford.edu/courses/2011/ph240/zhong2/.

3. Jake Christensen, Paul Albertus,Roel S. Sanchez-Carrera,Timm Lohmann,Boris Kozinsky, Ralf Liedtke, Jasim Ahmed, and Aleksandar Kojica ,Journal of The Electrochemical Society, (2012) ,159 ,(2), R1-R30.

4. G. Girishkumar,B. McCloskey, A. C. Luntz, S. Swanson, and W. Wilcke, Lithium-Air Battery: Promise and challenges, J. Phys. Chem. Lett, (2010), 1, 2193–2203.

5. Fujun Li, Hirokazu Kitauraand Haoshen Zhou, The pursuit of rechargeable solid-state Li–air batteries, Energy Environ. Sci., (2013), 6, 2302.

6. https://en.wikipedia.org/wiki/Lithium-ion_battery#Electrolytes.

7. Jiajun Wang, Yongliang Li, Xueliang Sun. Challenges and opportunities of nanostructured materials for aprotic rechargeable lithium–air batteries. Nano Energy (2012), 2 ,443-467.

8. F.Y. Cheng, J. Liang, Z.L. Tao, J. Chen Advanced Materials, 23 (2011), pp. 1695–1715
9. Yi-Chun Lu,Yang Shao-Horn, J. Phys. Chem. Lett. (2012), 4, 93-99.

10. Ian Kowalczk1, Jeffery Read2, and Mark Salomon.Pure Appl. Chem., (2007) Vol. 79, No. 5, pp. 851–860.
11. Min-Kyu Song,Soojin Park , Faisal M. Alamgir , Jaephil Cho,Meilin Liu,Materials Science and Engineering R 72 (2011) ,203–252.
12. Arumugam Manthiram. Materials Challenges and Opportunities of Lithium Ion Batteries. J. Phys. Chem. Lett. (2011) ,2, 176–184

13. Alexander Kraytsberg, Yair Ein-Eli. Journal of Power Sources 196 (2011) 886–893.
14. W. Xu, V.V. Viswanathan, D. Wang, S.A. Towne, J. Xiao, Z. Nie, D. Hu, J.-G. Zhang. Power Sources, 196 (2011), pp. 3894–3899.

15.W. Xu, K. Xu, V. Viswanathan, S.A. Towne, J.S. Hardy, J. Xiao, Z. Nie, D. Hu, D. Wang, J.G. Zhang J. Power Sources, (2011), 196 pp. 9631–9639

16. S.A. Freunberger, Y. Chen, Z. Peng, J.M. Griffin, L.J. Harwick, F. Bardè, P. Novak, P.G. BruceJ. Am. Chem. Soc., (2011), 133, pp. 8040–8047

17.T. Laino and A. Curioni, the Chemical Stability of Propylene Carbonate in the Presence of Lithium Peroxide, Chem. Eur. J., (2012) ,18, 3510.

18. Wu Xua, Kang Xub,Vilayanur V. Viswanathan. Journal of Power Sources (2011) ,196, 9631–9639.

19. Vyacheslav S. Bryantsev, Jasim Uddin, Vincent Giordani. Journal of The Electrochemical Society. (2012), 160(1):A160-A171.

20. Wu Xu,z Jie Xiao Deyu Wang, Journal of the Electrochemical Society, (2010), 157, 2, A219-224 ,.

21. Fuminori Mizuno, Kensuke Takechi, Shougo Higashi, Journal of Power Sources (2013) ,228,47-56.

22. Yuyan Shao, Sehkyu Park, Jie Xiao, ACS Catal. (2012), 2, 844−857.

23. Xiujing Lin, Lan Zhou, Int. J. Electrochem. Sci., 7 (2012), 9550 – 9559.

24. Yuhui Chen, Stefan A. Freunberger,Zhangquan Peng,Nature Chemistry,2013,5,1646.

25. Bard, A.J.; Faulkner, L.R.Electrochemical Methods: Fundamentals and Applications. New York: John Wiley & Sons, 1980.

26.http://www.cheng.cam.ac.uk/research/groups/electrochem/JAVA/electrochemistry/ELEC/l2html/l2mt.html.

27. Kosuke Izutsu, Electrochemistry in non-aqueous solution, Second edition. ISBN: 9783527323906

28.2.Jang-Soo Lee, Sun Tai Kim, Ruiguo Cao, Nam-Soon Choi, Meilin Liu, Kyu Tae Lee, Jaephil Cho, Adv. Energy Mater. (2011), 1, 34–50.

29. Cormac O. Laoire, Sanjeev Mukerjee, and K. M. Abraham. J. Phys. Chem. C *(*2010)**,** *114,* 9178–9186.

30. Cormac O. Laoire, Sanjeev Mukerjee, and K. M. Abraham. J. Phys. Chem (2009), 113, 20127–20134.